People`s Democratic Republic of Algeria
Ministry of Higher Education and Scientific Research

University of Echahid Hamma Lakhdar - El Oued
Faculty of Technology
Department of Mechanical Engineering

Dissertation

ACADEMIC MASTER

Domain: Science and Technology

Division: Electromechanical

Specialty: Electromechanical

Entitled

Realize an estimator of state of charge of electric vehicle battery

Dissertation Submitted in Partial Fulfillment of the Requirements for the Master Degree in electromechanical
Publicly defended in: 03/06/2024

Presented by:

- Ben Aoun Oussama
- Boughezala Ala Eddine
- Bouziane Kouraichi
- Ghendir Mohammed Bachir

Board of Examiners:

Mr. Djokhrab Ala Eddine	**Chairman**
Dr. Zine Bachir	**Supervisor**
Dr. Remha Souhaib	**Examiner**

2023/2024


بسم الله الرحمن الرحيم

Acknowledgement

first of all, we hold our thanks to **ALLAH** for giving us strength and courage

following we would like to warmly thank **Dr.zine bachir** our supervisor who has made enormous effort through his information,

and all **the professors of the department** of mechanical engineering to all those who were at one time or at any time involved in this work,

our warmest thanks to all those who from near and far have contributed to the realisation of this thesis

Dedicate

We humbly dedicate this thesis to our parents, whose unwavering support throughout our academic journey has been invaluable. Without their encouragement and sacrifices, the completion of this work would not have been possible.

This modest endeavor is also dedicated to our brothers and sisters, our extended family members, and all our loyal friends who have stood by us through thick and thin.

Moreover, we extend our gratitude to those individuals who have directly or indirectly contributed to the fruition of our efforts, their assistance has been instrumental in bringing this undertaking to its culmination.

Contents

Contents

List of Abbreviations and Symbols

List of Abbreviations

Abbreviation	Definition
EV	Electric vehicle
AEKF	Adaptive extended Kalman filter
Ah	Ampere-hour
ANN	Artificial neural network
ANFIS	Adaptive network-based fuzzy inference system
EKF	Extended Kalman filter
ELM	Elman neural network
EIS	Electrochemical impedance spectroscopy
AUKF	Augmented unscented Kalman filter
DKF	Dual Kalman filter
ELM	Elman neural network
MHE	Moving horizon estimation
NLO	Nonlinear observer
OCV	Open-circuit voltage
RLS	Recursive least square
SMO	Sliding mode observer
TNN	Transformer neural network
UKF	Unscented Kalman filter
SRRLS	Square root recursive least squares
EKBF	Extended Kalman–Bucy filter
ECMs	equivalent circuit models
PDEs	partial differential equations
SOC	State of charge
SOH	State of health

CC	Coulomb counting
BMS	Battery management system
RMSE	Root-Mean-Square Error
BMS	Battery management system
SVM	Support vector machine
SVR	Support vector regression
ECM	Electrical circuit model
$Li-ion$	Lithium-ion
$SOC0$	Initial State-of-Charge
RUL	Remaining Useful Life
SOP	State of power
VRLA	Valve Regulated lead acid bat
NiCd	Nickel-Cadmium
NiMH	Nickel-Metal Hybride
Li-PO	Lithium Polymer
LiCoO2	Lithium cobalt oxide
LiFePO4	Lithium iron phosphate
NMC	Lithium nickel manganese cobale oxide
h	hours
s	seconds
Cdo	Cadmium oxide

List of Symbols

Symbol	Definition	Unite
t	Time	[s]
T	Temperature	[°C]
$SOCend$	SOC indicated at the end	[%]
$SOC0$	SOC in the initial state	[%]
$SOCch$	SOC in the charge state	[%]
V	Battery voltage	[V]
Vd	Battery voltage after discharging	[V]
Vch	Battery voltage after charging	[V]
E	the initial cell voltage	[V]
Ra	the cell internal resistance	[Ω]
Qs	the instantaneous stored charge	
K	constant	
I	current	[A]
c	Concentration at the surface of the electrode	
OCV	Open-Circuit-Voltage	[V]
$n0$	Parameter related to the magnitude of the diffusion overpotential	
$n1$	Parameter related to the magnitude of the diffusion overpotential	[1/T]
$Vbat$	Battery terminal voltage	[V]
Qch	Amount of charge flowing into the battery during the charge state	[Ah]
Qd	Discharge capacity	[A]

List of Figures and Tables

List of Figures

List of Tables

General Introduction

General Introduction

In the context of the energy transition and the reduction of greenhouse gas emissions, electric vehicles (EVs) play a crucial role. One of the critical components for the functioning and performance of EVs is the battery, whose state of charge (SOC) must be accurately estimated to ensure optimal energy management. This thesis focuses on the realization of a state of charge estimator for the battery of an electric vehicle, employing both theoretical and experimental approaches.

The thesis is divided into three main chapters:

Chapter 1: State of the Art of Battery State of Charge Estimation in Electric Vehicles: this chapter explores the various existing techniques for estimating the SOC of EV batteries. We will discuss traditional and advanced methods, highlighting their advantages and disadvantages. Common approaches include voltage measurement, the coulomb counting method, empirical models, and techniques based on observation and modeling.

Chapter 2: Different Battery Models: in this chapter, we will present the different types of batteries used in EVs, with particular attention to theoretical and empirical models. Lead acid batteries, lithium-ion batteries, and other technologies will be examined. We will detail the characteristics of each model, their behavior under different charging and discharging conditions, and the key parameters affecting their performance.

Chapter 3: Experimental and Simulation Results, and Comments: this chapter is dedicated to presenting the results obtained from experiments and simulations. We will describe the test bench composed of various equipment such as the power supply, current and voltage sensors, LCD screen, Arduino board, a resistor as a load, and a 12V 7Ah lead-acid battery. Charging and discharging tests were carried out at different discharge currents (1C and 0.6C). The results will be analyzed and commented on, highlighting the effectiveness of the coulomb counting method and the empirical battery model.

The main objective of this thesis is to develop a reliable SOC estimator for EV batteries using a coulomb counting method combined with an empirical model. The experimental results will validate the proposed approach and discuss its practical implications for improving battery management systems in electric vehicles.

CHAPTER I

State of the Art of Battery State of Charge Estimation in Electric Vehicles

Chapter I: State of the art of battery soc estimation in Electric Vehicles

I.1 Introduction

In this chapter we will present some definitions of SOC, battery management system, and conventional and advanced battery estimation techniques including the Coulomb counting method and the hybrid method.

I.2 Battery Management System

The diagram labeled Figure I.1 depicts the typical architecture and components that comprise a Battery Management System (BMS). This system is designed to comprehensively monitor and manage the operational health and condition of a battery pack, formally termed the State of Health (SOH). The illustrated BMS layout consists of various integrated elements, including sensors to collect data, actuators to perform actions, control units to process information and make decisions, and communication channels to facilitate data transfer.

Enabling bidirectional communication between the central BMS control module and external interfaces like the human-machine interface is the Controller Area Network (CAN) communication bus protocol. Along with ensuring dependable function across both regular and irregular operational scenarios, a key responsibility of the BMS is to accurately determine and report the battery pack's state of charge data to the master Vehicle Control Unit (VCU) that oversees the vehicle systems.

A BMS that is engineered with robust and comprehensive design principles enables the real time acquisition of critical data parameters, encompassing electrical measurements, temperature readings, and other pertinent operational information, through the utilization of integrated sampling hardware components. The data collected by these hardware elements is then processed and analyzed employing sophisticated embedded algorithms and methodological approaches to derive accurate estimations of various battery condition states, such as SOC , SOH, SOP, and Remaining Useful Life RUL [1].

Ultimately, these derived battery state parameters are communicated and transmitted to the centralized Vehicle Control Unit (VCU) to facilitate optimal power management and distribution across the vehicle's systems.

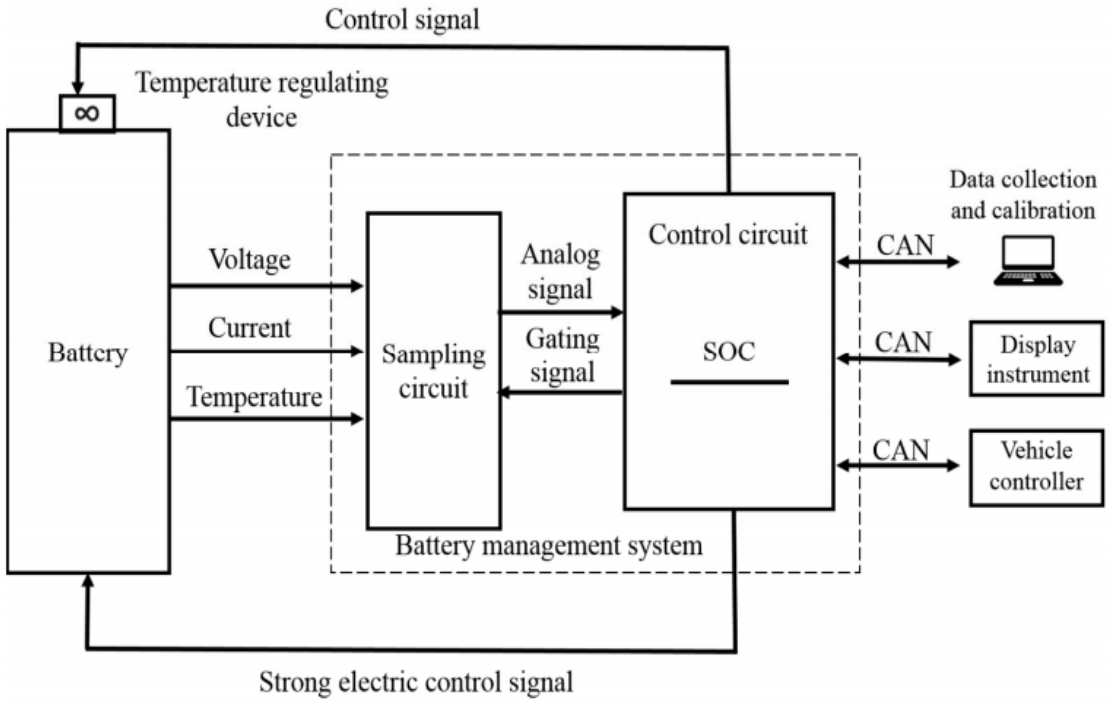

Figure I. 1. *BMS diagram [2].*

I.3 Definition of General Battery Parameters

To facilitate a discussion centered around eco conscious approaches to determining a battery's State of Charge (SOC), which indicates the remaining charge level, it is crucial to establish a shared understanding of frequently used terminology within this domain. Clarifying the definitions of common phrases and concepts related to SOC estimation techniques can foster a more productive and environmentally .responsible dialogue on this topic

Ampere-hour: A measure of electric charge defined as the essential product of current (in Amperes) and time (in hours).

Cell: The fundamental electrochemical unit employed to produce electrical energy from stored chemical energy or to store electrical energy in the form of chemical energy. A cell comprises two electrodes within a container filled with an electrolyte.

Battery: Two or more cells connected in a series or parallel arrangement to achieve the operating voltage and capacity needed for a specific load. The term is also commonly used for individual cells.

Li-ion cells: Cells that contain a liquid organic or polymer electrolyte, wherein both the anode and cathode are composed of intercalation compounds [3].

Cycle life: The number of cycles that a cell or battery can undergo charging and discharging under specific conditions before the available capacity in Ampere-hours (Ah) drops below certain performance criteria. Typically, this criterion is set at 80% of the rated capacity.

Cut-off voltage: The lowest operating voltage at which a cell is deemed depleted. This is also commonly referred to as end-of-discharge voltage or final voltage [4].

C-rate: A charge or discharge current, expressed in Amperes, equivalent to the rated capacity in Ampere-hours (Ah). Multiples larger or smaller than the C-rate are used to express higher or lower currents. For example, the C-rate is 1100 mA in the case of an 1100 mAh battery, while the C/2 and 2C-rates are 550 mA and 2.2 A, respectively.

Maximum capacity: The maximum amount of capacity that can be extracted from a battery under specified discharge conditions.

Capacity: The electrical energy stored in a battery, expressed in ampere-hours (Ah).

Self-discharge: During storage periods, batteries can experience a recoverable loss of usable capacity due to internal chemical reactions occurring within the cells. This phenomenon is known as self-discharge, and it is typically quantified as a percentage of the rated capacity that is lost over the course of one month at a specific ambient temperature. The rate of self-discharge is highly dependent on the temperature, as higher temperatures accelerate these internal reactions. The underlying mechanism behind self-discharge involves a localized redox process triggered by the decomposition of the electrolyte solution [3]. Additional significant contributing factors to self-discharge include the presence of micro-short circuits within the cell and the involvement of shuttle molecules that can transport charge between the electrodes.

Spread: Difference between characteristics of batteries of the same type.

State-of-Health (SOH): A "metric" that indicates a battery's current condition and its ability to deliver specific performance compared to a new battery.

State-of-Charge (SOC): The proportion of the maximum feasible cost currently stored within a rechargeable battery.

Depth-of-Discharge (DoD): The amount of power drawn from a battery, expressed as a percentage of its maximum capacity.

Depth-of-Charge (DOC): The amount of energy stored in a battery, expressed as a percentage of its maximum capacity.

Remaining run-time: The estimated duration for which a battery can provide power to a portable device under normal discharge conditions before it ceases to function.

I.4 State of the art of battery soc estimation technique

The State of Charge (SOC) refers to the proportion of available charge remaining in a battery compared to its maximum charge capacity when fully charged. It functions as a "fuel gauge," providing essential information for the safe operation of batteries.

Many different methodologies have been presented in the scientific literature to estimate the load, health and operational status of EV batteries [5]. Among the various algorithms and models developed to estimate battery state of charge (SoC), some methods are distinguished by either the simplicity of their implementation or the complexity of their structures [6].

The review classifies different approaches to state-of-charge (SoC) estimation as shown in Figure I.2. Traditional methods typically rely on indirect estimation of state of charge by incorporating several physical characteristics of the battery, such as voltage levels, current flow, internal resistance, operating temperature, and total impedance measurements [7,8]. For example, by accurately determining the critical parameters of the battery pack, an improved control and diagnostic system can be developed, ensuring the safety and durability of the battery [9].

To implement state-of-charge (SoC) estimation techniques based on adaptive filters, nonlinear observer models can be used in complex and nonlinear systems [6]. Learning algorithms include computational intelligence methods, including fuzzy logic, neural networks, and biological optimization algorithms. The hybrid approach is to combine two or more of these techniques to improve the accuracy of state of charge (SoC) estimation [6].

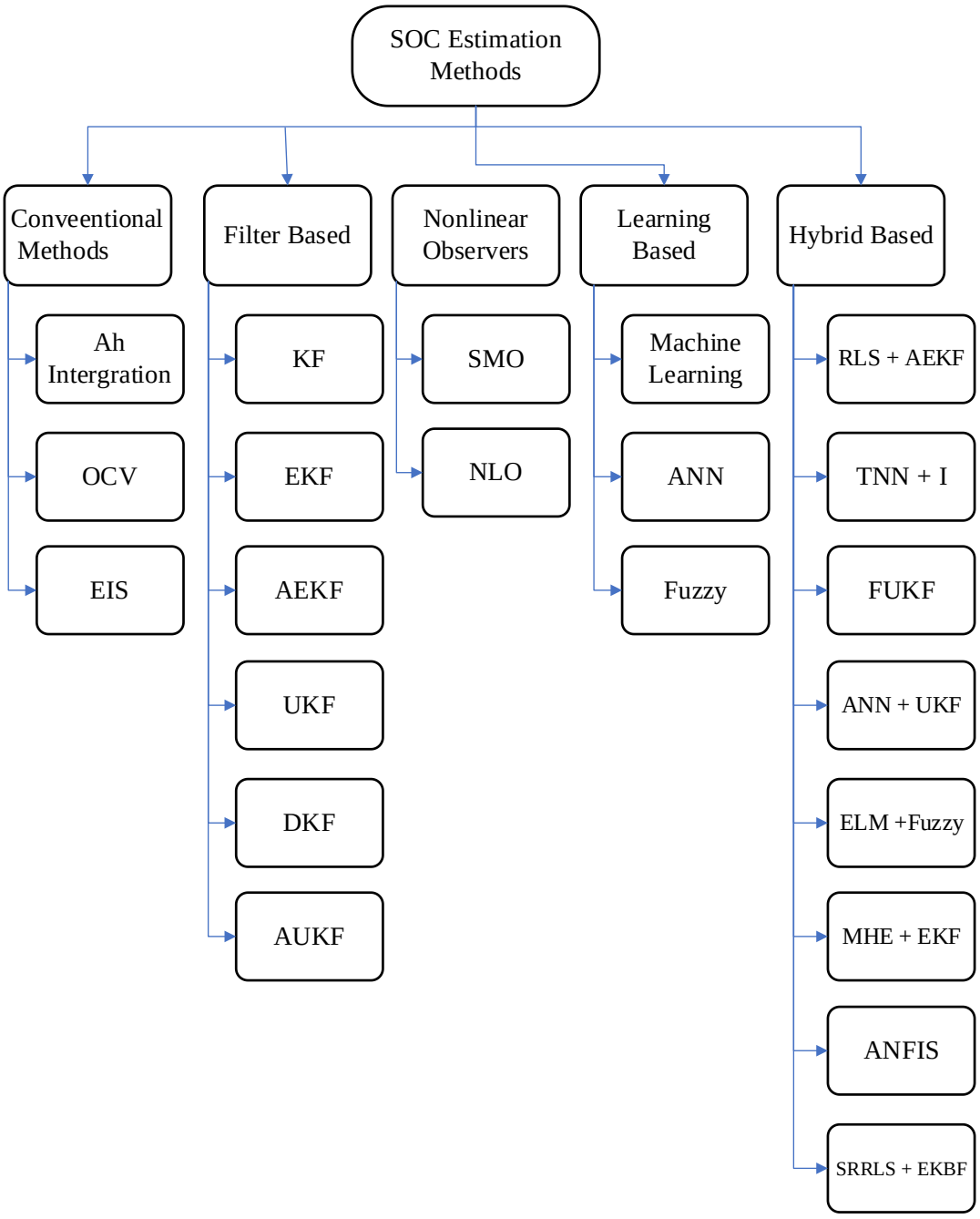

Figure I.2: *Categorizing the Various Approaches for Estimating the State of Charge.*

I.5 Conventional Methods

One widely used technique for SOC estimation is the coulomb counting (CC) method. This approach factors in the charging or discharging current of the battery by integrating it over time to determine the SOC level. The coulomb counting methodology allows for the incorporation and modeling of various internal battery dynamics and phenomena that affect SOC, such as self-

discharge rates, capacity fade loss over time, and discharge efficiency factors [10]. The mathematical formulation [14] that describes this SOC estimation approach is given by:

$$\mathbf{SOC} = \mathbf{SOC_0} - \frac{\mathbf{1}}{\boldsymbol{C_N}} \int_{t0}^{t} \boldsymbol{\eta} \cdot \boldsymbol{I}(\boldsymbol{\tau}) \boldsymbol{d\tau} \qquad (\boldsymbol{I}.\mathbf{1})$$

where SoC(t0) represents the initial SoC value; T is the sampling period; CN denotes the nominal battery capacity; η stands for the Coulomb efficiency; i(t) signifies the charging/discharging current; and Sd indicates the self-discharge rate. Accurate determination of the initial state of charge value is very important and ensures an error and uncertainty free phase throughout the estimation process.

The coulomb counting method is not usually used alone to estimate the state of charge, but is combined with other modern techniques for the purpose of improving accuracy. In [12], the accuracy of the coulomb counting method is affected by the internal resistance of the battery.

However, estimating the real time state of charge by directly using the coulomb counting method is not entirely suitable [13].

I.6 Advanced techniques

I.6.1 Estimation Techniques Utilizing Filtering Algorithm Methodologies

The Kalman filter (KF) algorithm is an iterative optimal solver for linear systems in which process and measurement noise follow an independent normal distribution. However, this algorithm faces challenges when applied to nonlinear systems such as batteries. To address this shortcoming, various extensions to the Kalman filter have been proposed including extended Kalman filter (EKF), sigma point Kalman filter (SPKF), unbiased Kalman filter (UKF), and central difference Kalman filter (CDKF). These extensions have been widely employed to estimate the state of charge (SOC) of batteries with nonlinear characteristics [14,15].

One study [16] showed that using modified open circuit voltage correlation (OCV-SOC) and measurement noise models with extended Kalman filter (EKF) enabled more robust estimates of SOC for battery cells. The EKF's ability to balance complexity and accuracy also makes it suitable for implementation in battery management systems (BMSs). However, EKF plots non-linear properties, which introduces layout errors.

To address this, the researchers proposed a sigma point Kalman filter (SPKF) that showed higher estimation accuracy than EKF without significant additional computational costs [17]. Comparative studies have shown that SPKF and its extensions such as CDKF and UKF have higher robustness against uncertainty and better convergence behavior compared to EKF [18]. These filters have been applied with battery models to obtain accurate SOC estimates while reducing computational time.

An accurate knowledge of process and measurement noise variations is crucial to all Kalman filter extensions. Incorrect estimates of these variances can lead to large errors in the estimated results. To address this challenge and adaptively match noise variations in real time, adaptive Kalman filter based estimation methods such as adaptive extended Kalman filter (AEKF) and adaptive unbiased Kalman filter (AUKF) have been applied to estimate the SOC of batteries.
However, a problem arises from the assumption that process and measurement noise are normally distributed in these stretches, an assumption that may not be consistent with realistic scenarios, which may affect the convergence behavior and accuracy of the estimates [19-22].

I.6.2 Estimation Approaches Leveraging Nonlinear Observer Models

I.6.2.1 State Estimation via Sliding Mode Observation Techniques

SMO, or Sliding Mode Observer, serves as an enhanced training controller designed to ensure the robustness and stability of a system in the presence of model uncertainties and environmental disturbances. SMO is constructed by incorporating the state equation into the subsequent stage, which is then decayed to the observer queries. In [22] A refined version of SMO was introduced to manage the nonlinear dynamic characteristics of batteries by incorporating an RC circuit. This approach offers a controller capable of handling the complex discharge and charge rate transitions. Validation was conducted using the UDDS, and the results indicated an SOC error of less than 3%. In [23] , The Adaptive Gain Sliding Mode Observer (AGSMO) algorithm was employed to estimate the battery State of Charge (SOC) based on a combined equivalent circuit model.

To define the constraints, a battery pulse was utilized, and state equations were formulated by incorporating the circuit model along with terminal voltage data. Experimental trials were conducted to evaluate the proposed methodology, and the results demonstrated that the model offers an advantage in regulating the robustness associated with various operational conditions.

I.6.2.2 State Estimation Employing Nonlinear Observer Models

Multiple observers have been employed, encompassing both linear observers [24–26] additionally, a nonlinear observer [27] was utilized to estimate the SOC. In [28], The SOC estimation based on Nonlinear Observer (NLO) dependency was introducced using a first order corresponding RC circuit model. This model was validated using a driving cycle and discharge test data, demonstrating improved performance in terms of speed, precision, and cost compared to extended Kalman Filter (KF) and Sliding Mode Observer (SMO). However, researchers are still exploring an optimal gain matrix to further reduce estimation errors.

I.6.3 State of Charge Estimation Approaches Utilizing Learning AlgorithmTechniques

I.6.3.1 State of Charge Estimation via Artificial Neural Network Models

An NN, or Neural Network, is both a self learning algorithm and an intelligent tool. It leverages trained data to estimate the state of charge without requiring prior knowledge of the initial state of charge data. Typically, it comprises input, hidden, and output layers, forming a structured NN architecture, as depicted in Figure I.3 [29]. Constructing the NN structure involves utilizing discharge current, temperature, and voltage as inputs, while the SOC serves as the output. An NN offers the advantage of being adept at handling nonlinear battery conditions. However, it comes with certain drawbacks, including the necessity for a substantial volume of data for training purposes and the requirement for significant memory capacity to store this information [30,31].

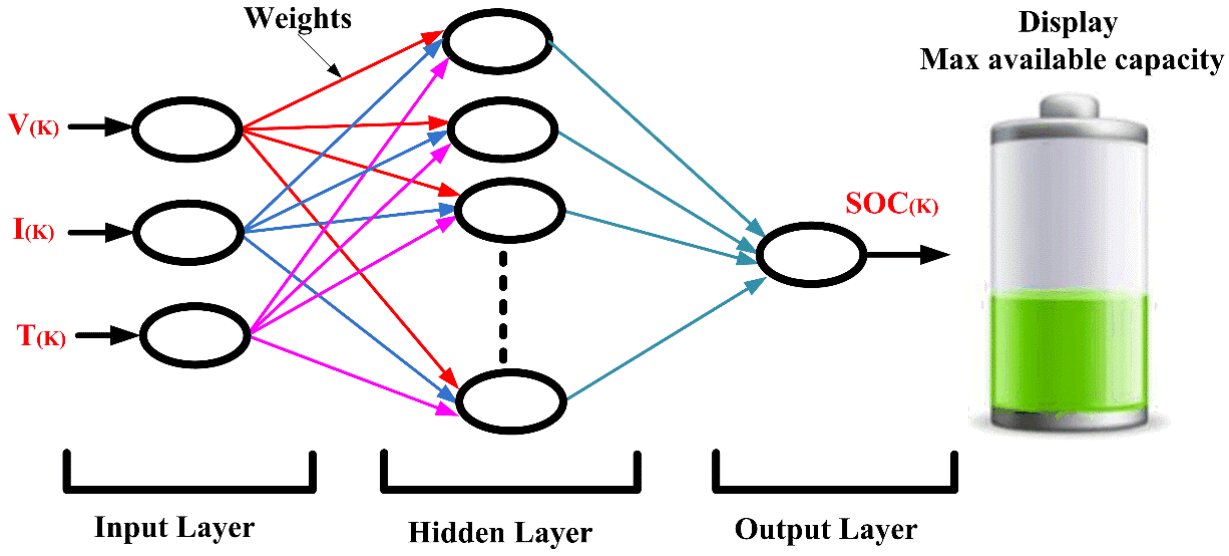

Figure I.3: *Overall structure of neural network for SOC estimation [29].*

I.6.3.2 State of Charge Estimation via Fuzzy Logic Algorithm

Fuzzy logic (FL) is recognized as a powerful algorithmic methodology for modeling nonlinear and complex systems by leveraging training data. Its implementation involves the use of rule based mapping of inputs to outputs, reasoning based on membership function definitions, and defuzzification techniques to obtain crisp output values. However, estimating nonlinear models using FL can be computationally intensive, often requiring complex calculations, dedicated hardware processing units, and substantial memory resources. Despite these challenges, FL remains a valuable tool for handling nonlinearities and uncertainties in various application domains.

Researchers have explored the application of fuzzy logic techniques for estimating the state of charge (SOC) of batteries by utilizing data obtained from constant current (CC) testing methods. This approach utilizes three input variables sampled at different frequencies, including impedance measurements and the SOC itself, with the aim of predicting the SOC with a maximum error margin of ±5%. Studies have shown that advanced adaptive neuro fuzzy inference systems (ANFIS), which combine fuzzy logic with neural network architectures, are particularly effective for SOC estimation in lithium-ion batteries. ANFIS based methods have been extensively investigated and implemented in various battery management applications [33-38].

The work by Salkind et al. [32] highlights the potential of fuzzy logic techniques for modeling nonlinear and complex systems, such as battery state estimation, by leveraging training data. However, the authors also acknowledge the computational complexity and resource requirements associated with implementing these techniques, particularly for real-time applications.

I.6.3.3 State of Charge Estimation Using Genetic Algorithm Optimization Techniques

Genetic algorithms are a class of optimization techniques primarily employed for determining optimal parameter values and configurations. Their fundamental functionality involves iteratively modifying the constraint handling mechanism and solution candidates to enhance the overall efficacy and quality of the solution approach.

These algorithms have found widespread applications across various domains, including mathematics, physics, and engineering disciplines, particularly in solving nonlinear optimization problems to identify ideal parameter configurations. In the context of battery SOC estimation,

Zheng et al. [39] employed a genetic algorithm to optimize the SOC estimation for four LiFePO4 battery cells arranged in a series configuration. Remarkably, the outcome of this genetic algorithm based method resulted in an SOC estimation error of less than 1%, showcasing its effectiveness in accurately determining the state of charge for the battery system under study.

Xu et al. [40] also explored the use of genetic algorithms for battery SOC estimation problems, further highlighting the potential of these optimization techniques in this domain. Genetic algorithms' ability to navigate complex solution spaces and identify optimal parameter settings make them a valuable tool for enhancing the accuracy and robustness of battery SOC estimation methods.

It is important to note that while genetic algorithms can effectively solve nonlinear optimization problems and lead to accurate SOC estimation results, their implementation may involve substantial computational resources and time, particularly for large scale or real time applications. Consequently, trade offs between estimation accuracy, computational complexity, and practical implementation constraints need to be carefully evaluated when employing genetic algorithms for battery SOC estimation tasks.

I.6.3.4 State of Charge Estimation via Support Vector Machine Modeling

The Support Vector Machine (SVM) algorithm is primarily a regression algorithm that operates on a Kernel mission. Its goal is to transform nonlinear relationships in inferior measurements into linear representations in higher dimensional spaces. In [41], The SVM technique was employed for SOC estimation, utilizing independent variables such as current, temperature, and voltage to define model constraints even during battery discharge or charging cycles. This approach was validated, achieving a high level of SOC precision with an estimated quantity of 0.97. SVM offers advantages in handling high dimensional models and nonlinear relationships. With the aid of training data, SOC estimation can be performed swiftly and accurately. However, a drawback of this method the need to engage in trial and error methods, which can be time consuming [42].

I.6.4 Hybrid Methods

combined synergistically to leverage the strengths of each individual algorithm employed together to amplify their collective capabilities the effectiveness and accuracy of the battery model. This method not only yields reliable and efficient results but also reduces the cost of the battery

management system [43,44]. However, this technique involves highly complex mathematical calculations that require a substantial memory device to be incorporated [45]. A nonlinear system, such as a LiB, may possess unknown model parameters that need to be identified utilizing the genetic algorithm (GA), an optimization technique inspired by biological processes. The GA initiates a random set of chromosomes and employs biological operations such as crossover, selection, and mutation to ascertain the optimal values. Additionally, the second-order ECM parameters of a battery were determined utilizing the GA [46-51].

The bacterial foraging algorithm (BFA) is an optimization method inspired by nature and modeled after the cooperative foraging behavior of Escherichia coli bacteria. Renowned for its simplicity and high efficiency, the BFA has been effectively employed to tackle a wide array of technical and mathematical challenges [52,53]. The unknown properties of LiB were also estimated using the Bacterial Foraging.

Algorithm (BFA) [54]. In PSO (Particle Swarm Optimization), a nature inspired algorithm is utilized to find the optimal solution to complex engineering problems. This approach is similarly employed by [55-64] to find the unknown parameter of LiB with model based SoC estimation.

I.7 Comparative Analysis

Table I.1 shows us some state-of charge methods and examines their advantages and disadvantages, important considerations and limitations

Table I.1: Methods for estimating charge status [6,65-70].

Charge Estimation Methods	Advantages	Disadvantages	Considerations and Limitations
Conventional Methods	A manual approach can suffice instead of developing an algorithm for implementation.	The battery was required to remain in an inactive or low-power state for an extended duration.	Researchers who didn't report mistakes often performed simulations or empirical assays to corroborate the validity of their methodological approaches. With regard to the hybrid algorithm, the obtained results stemmed from physical experiments involving an embedded algorithmic implementation.

Kalman Filter-Based	The precision level is satisfactory for the intended purpose. The system has the capability to handle irrelevant or redundant data.	Developing an adequately precise battery model necessitates substantial computational resources, including prolonged processing times and extensive memory usage, as well as the implementation of an intricate algorithmic procedure.	The precision of the methodological approach is contingent upon the fidelity of the battery model employed. Such procedural paradigms necessitate an extended execution duration and augmented memory capacity, attributable to the elevated complexity inherent in their algorithmic formulations.
Nonlinear Observed Based	The model demonstrates satisfactory precision and an ability to cope with uncertainties or inconsistencies in the modeling process.	The intricate nature of the computational algorithm poses difficulties for its practical utilization in real time or online applications.	Despite conducting physical tests, the authors found that nonlinear methods are challenging to apply online due to the complexity of the algorithm.
Learning Based	The system possesses a robust capability to estimate complex nonlinear functions with a high degree of accuracy.	To ensure the algorithm's effectiveness across all operating scenarios, the training process necessitates the acquisition and utilization of a substantial volume of data, encompassing a diverse range of conditions.	The proposed methodology exhibits versatility, applicable across the entire spectrum of operational conditions. However, its implementation mandates the procurement of a substantial volume of data to facilitate the training of the algorithmic model. Furthermore, this approach demands an elevated level of computational processing time, consequently incurring higher associated costs.
Hybrid-Based	While decreasing the overall system cost, these methods simultaneously enhance the accuracy and dependability of the estimation outcomes.	Integrating multiple methodologies constitutes an arduous undertaking that necessitates intricate computational procedures.	The integration of the two methodological approaches synergistically augments the precision and fidelity of the overall system.

From the table, we notice that the hybrid method is the best, although it is complex, but it is more accurate, effective, and less expensive for the system.

I.8 Conclustion

In this chapter, we talked about the literature review of conventional and advanced techniques for estimating the state of charge of batteries. After in depth study and careful comparison, we chose the easier technique, which is coulomb counting, for the reason of its simplicity and ease of application.

CHAPTER II

Different Battery Models

Chapter II: Different Battery Models

II.1 Introduction

In this is chapter, we will discuss battery charging and its various models. We will talk in detail about lead acid batteries and lithium-ion batteries, study the disadvantages and advantages, and determine the best among them.

II.2 Electric Vehicle Battery Technologies

II.2.1 Overview

Today, electric vehicles (EVs) have garnered significant interest due to the imperative to curb automobile emissions. The efficient utilization of energy and the preservation of the global environment have become matters of public concern. A current focus lies in equipping efficient electric power infrastructure to mitigate air pollution, particularly reducing CO2 emissions [71].

The battery technology stands as a cornerstone in the development of electric vehicles (EVs). Several countries, including the United States, Japan, and Germany, have initiated dedicated projects aimed at enhancing battery performance to meet the demands of EVs. Over the years, battery cell performance has shown remarkable advancements, reflecting continuous improvement [72].

In recent times, rechargeable lithium-ion (Li-ion) batteries have emerged as the most suitable energy storage solution for electric vehicles (EVs). This is attributed to their superior attributes including higher energy density and specific power, lighter weight, lower self discharge rates, greater recyclability, and longer cycle life compared to lead acid, nickel cadmium (NiCd), and nickel metal hydride (NiMH) batteries [72-74].

II.2.2 Basics of Lead Acid Battery

Lead acid batteries remain one of the most popular and enduring technologies in the realm of batteries. Even in modern times, they uphold a reputation for high reliability and affordability, owing to their mature technology [75]. Disadvantages of this technology include low specific energy and a relatively short service life [76]. Furthermore, lead acid batteries dominate the global battery market, accounting for 65% of it. This is due to their widespread use in wide areas such as automated vehicles and storage of generated energy.

Lead acid batteries stand out as one of the most prevalent secondary battery types, mainly employed for storing substantial cell potential. They are prominently utilized in automotive engines. Their benefits encompass low cost, high voltage, and significant cell potential storage capacity. However, they suffer from drawbacks such as heavy weight, inefficiency in low temperature conditions, and inability to retain their potential over prolonged periods of disuse [77, 78].

The reactions of a lead acid battery are illustrated below:

During discharging, which happens when the load is connected, the cell potential reaches 2.02V. Consequently, charging takes place when the car is in motion, and the electrode potential reaches -2.02V. This constitutes a non spontaneous reaction necessitating an external electrical source. The reverse reaction occurs during charging. Table II.1 depicts the chemical state of a charged and discharged lead acid battery:

Table II.1: The chemical state of Lead Acid Battery [79].

	Anode	***Electrolyte***	***Cathode***
Fully Charged	Pb	H_2SO_4	PbO_2
Fully Discharged	$PbSO_4$	H_2SO_4	$PbSO_4$

II.2.3 Basics of Lithium-ion Battery

Lithium-Ion (Li-ion) technology represents one of the latest advancements in battery technology, continually undergoing research and development. Among various battery technologies, Li-ion holds significant promise for electric vehicles (EVs) due to its high specific energy, high voltage operation, and extended cycle life. However, challenges persist, notably the high initial cost and susceptibility to degradation from deep discharge cycles and temperature fluctuations [80-81]. Lithium-ion batteries have become ubiquitous in our daily lives, with most of us carrying one in our phones. There are several types of lithium-ion batteries, distinguished mainly by their cathode chemistry, including:

- Cobalt-based lithium oxide compound (LiCoO2)

- Iron phosphate lithium compound (LiFePO4)

- Manganese oxide lithium compound (LiMn2O4)

- Lithium-polymer composite

- Nickel manganese cobalt oxide lithium compound (LiNiMnCoO2 or NMC)

Each type offers different characteristics, with trade offs between cost, efficiency, and safety. Lithium-ion batteries are prized for their light weight (6.94g/mol) and high energy density (3860 mAh/g), a feature that has been studied since the 1950s. However, commercial Li-ion batteries only emerged in the late 1990s. Today, various varieties are available, with Lithium-ion (Li-ion) and Li-polymers (Li-Po) being the most commonly used. Terminal voltage typically ranges from 3 to 4.2V. Figure II.1 depicts a diagram of a LiCoO2 variation within the lithium-ion family.

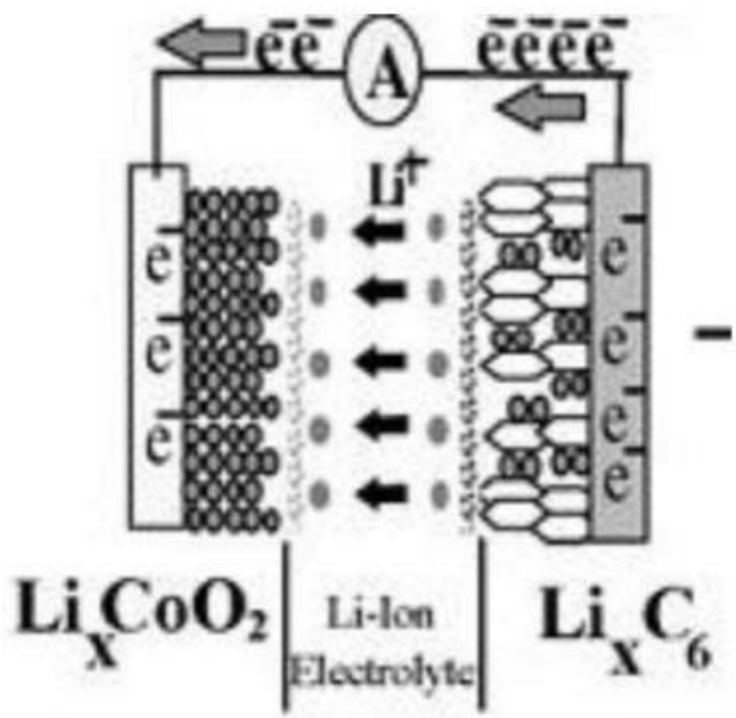

Figure II.1: *The Electrochemical Reaction Mechanism in Lithium-Ion Batteries [82].*

Lithium-ion batteries are characterized by many chemical compositions, so they are divided into two types: lithium iron phosphate (LFP, LiFePO4) and metal oxide compounds (such as NCM, NCA, cobalt, and manganese) [83]. Table II.2 represents the difference between them in the cell.

Table II.2: Lithium-ion Subcategory Comparison [84, 85].

	LFP	LiNCM
Voltage	3.3 V nominal (2-3.6 V/cell)	3.7 V nominal (2.7-4.2 V/cell)
Energy Density	300 Wh/L	735 Wh/L
Specific Energy	128 Wh/kg	256 Wh/kg
Power	1000 W/kg	512 W/kg
Cycle Life	2,000 @ 100% DoD 3,000 @ 80% DoD	750 @ 100% DoD 1,900 @ 80% DoD
Calendar Life	6 years	8 years
Max recommended temperature	40°C	55°C
Safety	High	Moderate
Commercial Suppliers	A123, Valence, BAK, BYD, K2, Lishen, many Chinese vendors	Sanyo, Panasonic, Samsung, DowKokam, Sony, LG Chem, Moli

Indeed, all lithium-ion cells are considered "deep cycle," implying their capability for full charge and discharge cycles. To enhance the battery's lifespan, it's advisable to limit the depth of each discharge to approximately 80% of the rated capacity. This practice can significantly extend the battery's life.

II.3 Methods of Charging Electric Vehicle Battery

II.3.1 Constant current

The methodology of constant current charging necessitates the modulation of either the charging devices' output voltage or the resistive element placed in series with the battery, with the explicit purpose of maintaining a consistent flow of electric current. This approach ensures a uniform current level throughout the duration of the charging process. In the case of nickel-cadmium battery technologies, which exhibit a propensity for polarization during conventional charging protocols, both the traditional constant voltage and constant current charging techniques culminate in the persistent generation of hydrogen-oxygen gaseous byproducts within the electrolytic medium. Consequent to elevated internal pressures, the oxygen molecules undergo migration towards the negative electrode, initiating a chemical reaction with the cadmium plate, thereby resulting in the formation of cadmium oxide (CdO) and an attendant reduction in the effective capacity of the electrode plate. As the battery's acceptable current capacity undergoes a gradual diminution during the charging cycle, this phenomenon can precipitate overcharging during the latter stages of the process. Ultimately, such overcharging can engender a significant degradation in the battery's overall capacity over an extended temporal span [86].

II.3.2 Constant Potential Charging

Industrial settings commonly employ modified constant potential charging techniques. The modified constant charging capacity approach finds applications across various domains such as vehicular transportation, power grids, telecommunications systems, and uninterruptible power supplies, where the charging circuit connects directly to the battery unit. In these setups, the charging circuit enforces a current limitation, maintaining this level until reaching a predetermined voltage threshold. Beyond this point, the voltage remains fixed until battery discharge occurs. Appropriately determining the current limit and constant voltage level proves critical, typically based on the duration the battery sustains a 100% charge state. Selecting a lower charging current proves advantageous to circumvent issues like overloading, grid corrosion, electrolyte water depletion via electrolysis, and the associated maintenance needs to replenish lost water during this "float" mode of operation while under load. To fully recharge at a low constant potential, adhering to the manufacturer's specified initial current ratings becomes essential [87].

II.4 Types of Battery Models

II.4.1 Lead Acid Battery Models

Various modeling techniques exist for lead-acid batteries [88], including electrochemical models, computational fluid dynamics models, finite element models, and electrical equivalent circuit models. To develop these models, experimental data is required to characterize battery behavior and generate response curves by measuring voltage and current during both charging and discharging operations. While electrochemical, computational fluid dynamics, and finite element models provide valuable insights into battery technology fundamentals, they are not ideally suited for simulating the real world performance of battery devices. On the other hand, the electrical equivalent circuit modeling approach uses electrical equations to represent different battery parameters and characteristics, making it advantageous for simulating and analyzing the actual behavior of battery devices.

The study of various models progresses from a basic representation of a battery to more intricate models. This research aims to gain a comprehensive understanding of the electrical behavior of batteries. Consequently, the following are different models of electrical batteries:

a) Simple Battery Model

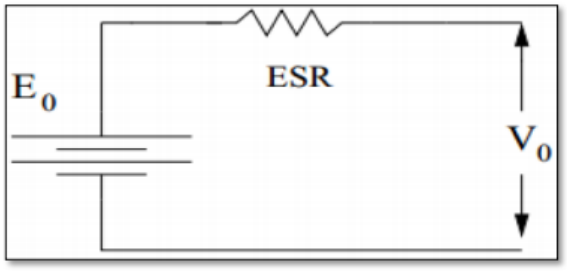

Figure II.2: *Analogous Circuit Representation of a Rudimentary Modeling Approach [89].*

b) Thevenin Battery Model

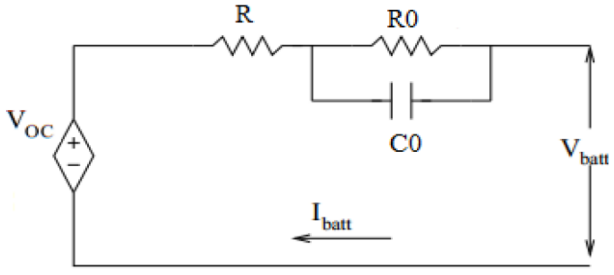

Figure II.3: *Analogous Circuitry Formulation Based on the Thevenin Equivalent Model [90].*

c) **Copetti Model**

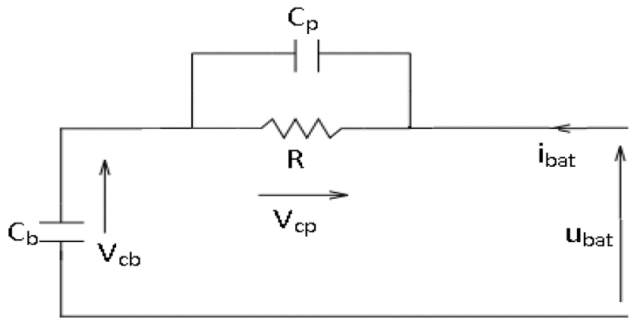

Figure II.4: *Analogous Circuit Representation of the Copetti Modeling Methodology [91].*

II.4.2 Lithium Battery Model

a) Equivalent Circuit Model

The analogous circuit model serves as a valuable tool for simulating the intricate properties of batteries. This model incorporates circuit components like resistors, capacitors, and a constant voltage source. It proves versatile across various battery operating conditions, allowing for the derivation of state-space equations to facilitate thorough study and practical application. Moreover, this model finds widespread use in simulation modeling and battery management systems across diverse electric vehicle platforms.

b) Simple Resistance (*Rint*) Model

The Rint model depicted in Figure II.5 represents the most basic equivalent circuit model for batteries. It consists of an ideal voltage source and a resistance, denoted as R0. R0 typically varies according to the state of charge (SOC), temperature, and operational modes (charging or discharging), determined through Hybrid Pulse Power Characterization (HPPC) tests [92].

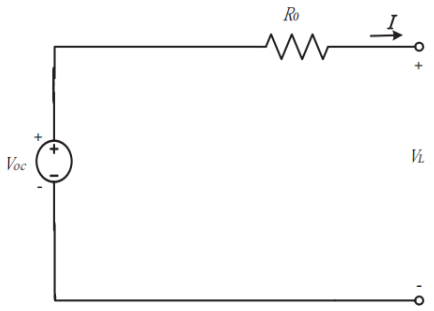

Figure II.5: *Schematic Representation of the Analogous Circuit for the Internal Resistance (Rint) Modeling Approach.*

c) RC Model

Table II.6 shows the resistor-capacitor (RC) model, where Rt represents the resistance associated with the tip, Re with the bulk solution, and Rc with the surface. Cb denotes the battery's capacity for chemical charge storage, while Cc, possessing a relatively low value, accounts for surface effects within the battery [92].

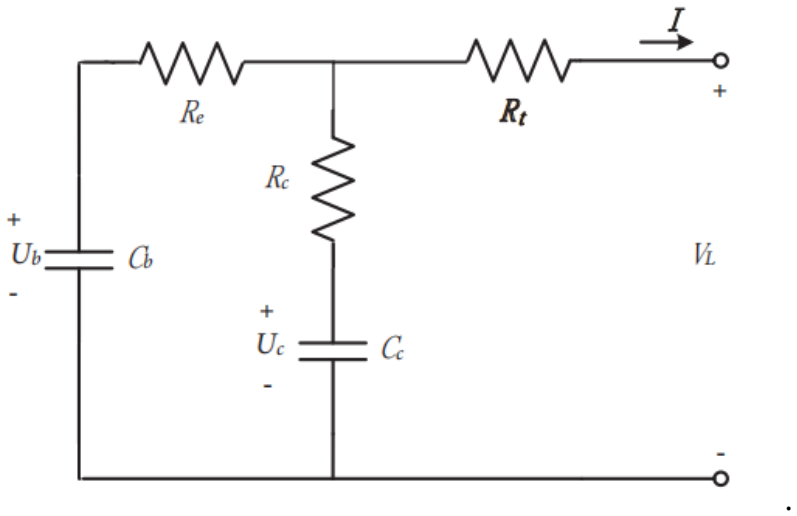

Figure II.6: *Schematic Depiction of the Equivalent Circuit for the Resistor Capacitor (RC) Modeling Methodology.*

d) Thevenin Model

The figureII.7 or drawing represents thevenin model such that:

- E_0 open circuit voltage.

- R_0 internal resistance

- I(t) the charging or discharging current

- V(t) the terminal voltage of the battery

In addition, the RC circuit inside the model characterizes the battery polarization phenomenon [93].

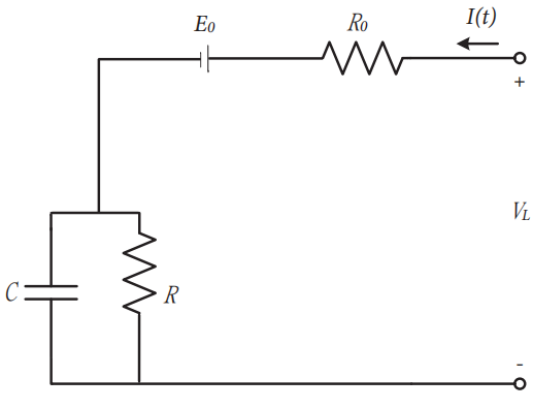

Figure II.7: Thevenin model equivalent circuit diagram.

e) DP Model

While a single RC component, like in Thevenin's model, can approximate polarization effects, its accuracy diminishes towards the end of charge or discharge cycles. The Dual Polarization (DP) model, depicted in Figure II.8, enhances polarization characterization by separately simulating concentration and electrochemical polarization effects. Within this model, Rpa and Rpc denote electrochemical and concentration polarization, respectively. Additionally, Cpa and Cpc represent the transient response during power transfer for electrochemical and concentration polarization, respectively [92].

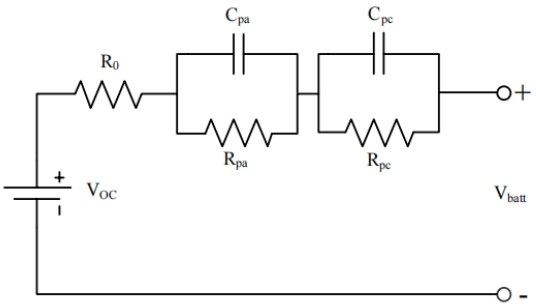

Figure II.8: DP model equivalent circuit diagram

f) Electrochemical Model

Based on electrochemical theory [82]. The chemical model describes the battery reaction process through mathematical equations. The most common Pukert formula is known. Equation II.1 shows us that the relationship is not direct between the available charge and the discharge current (as one increases, the other decreases).

$$I^n T_i = Constant \quad \text{(II.1)}$$

where I is the discharging current, n the constant of a battery, and T_i is the discharging time under current I.

Equation II.1 expresses the Shepherd model, while voltage and current describe electrochemical activities [87].

$$E_t = E_O - R_i - K_i \left(\frac{1}{1-f}\right) \quad \text{(II.2)}$$

Et is the terminal voltage of a battery, EO the open circuit voltage of a fully charged battery, Ri the ohmic internal resistance, Ki the polarization resistance, $/$ the transient current and f the net discharging capacity calculated according to the Ah integration method.

Most of the time, the analysis of hybrid cars is based on the Shepherd model, in addition to calculating the SOC and battery voltage with the Peukert equation.

The shepherd model can find the tipping point where the terminal voltage starts to drop rapidly. Such a critical condition sometimes occurs during the actual operating cycle of an electric vehicle battery.

Unnewehr and Nasar give us a simplification of the shepherd model in equations II.2–II.4:

$$Et = EO - Ri - Kif \quad \text{(II.3)}$$

$$EOC = EO - Kif \quad \text{(II.4)}$$

$$R = RO - KRf \quad \text{(II.5)}$$

where EOC is the open circuit voltage, RO the total internal resistance of a fully charged battery, KR the experimental constant, and R the battery equivalent resistance.

It is developed into the Nerst model and the Nerst expanded model based on the Unnewehr model, respectively expressed in Equations II.4 and II.6.

$$Et = Ei - RiI - Ki \ln(f) \quad \text{(II.6)}$$

$$Et = EO - RiI - Ki \ln(f) + Kj \ln(1\_f) \quad \text{(II.7)}$$

Dr. Gregory L. Plett of the University of Colorado collectively formulated the three electrochemical models mentioned above Based on the Shepherd model, the Unnewehr model and the Nerst expanded model, seen in Equation II.7.

$$U_L = K_O - RI_L - \frac{K_1}{SOC} - K_2 SOC + K_3 \ln(SOC) + K_4 \ln(1 - SOC) \quad \textbf{(II.8)}$$

where UL is the battery loading voltage, IL the current, R the battery internal resistance, and K0, K1, K2, K3, and K4 are the mean model coefficients, respectively.

II.5 Comparing Lithium-ion and Lead Acid Batteries

The following table II.3 represents a comparison between lead acid and lithium-ion batteries and a study of their advantage and disadvantage.

Table II.3: Advantages and Limitations of Lead Acid and Li-ion Batteries [94-98].

	Lead Acid	**Lithium -Ion:**
Advantage	- Its price is low and economical - It is characterized by maturity and development so that it can be relied upon. - Convenient charging - Can be easily maintained - It has the ability to store energy.	- Light weight - It stores energy very efficiently - It has a longer life than other batteries - Fast shipping - Does not require complete emptying for maintenance
Disadvantage	-Heavy in weight and not suitable for some work -Its life is short and cannot be stored after unpacking -When the temperature rises, it does not work well -It causes harm to the environment due to its chemicals	-It's expensive -When the temperature rises, it does not work well -You need to take good care to avoid mistakes during shipping - Its performance weakens after use over time

We note from the table that lithium-ion batteries are better than lead acid batteries, especially in their age.

a) Additional comparison Table:

The following table II.4 represents a comparison between electrochemical battery models and experimental battery models and a study of their advantages and disadvantages, describing them:

Table II.4 Comparing between electrochemical battery models and empirical battery models [99-102].

	Description	**Advantages**	**Disadvantages**
Electrochemical Battery Models	Electrochemical battery models are founded on fundamental electrochemical principles that dictate the behavior of battery cells. They entail intricate mathematical equations that replicate the processes transpiring within the battery, including ion diffusion, electrode reactions, and charge transfer kinetics.	Offering comprehensive insights into the internal mechanisms of the battery, enabling precise performance forecasting across varying operational scenarios. This information can be leveraged for optimizing designs and developing control algorithms.	Demands a thorough understanding of battery chemistry and parameters, resulting in computationally intensive and frequently intricate implementations. Often necessitates experimental data for parameter calibration.
Empirical Battery Models	Empirical battery models rely on experimental data and statistical analysis instead of fundamental electrochemical principles. They employ mathematical equations or algorithms to depict the correlation between input and output variables, frequently derived from curve fitting techniques.	Straightforward to implement and computationally efficient, this approach can offer precise forecasts of battery performance utilizing existing experimental data.	These models often lack deep physical insights into battery operation and might struggle to generalize effectively beyond the range of training data. Consequently, they offer limited utility for understanding underlying mechanisms or optimizing designs.

From the table, we notice that the electrochemical battery models are better than the experimental battery models, despite their complex processes, but their results are accurate.

b) Cycle Life Comparison

In deep discharge applications, lithium-ion batteries indeed exhibit substantially higher cycle life compared to lead acid batteries. This discrepancy becomes more pronounced with rising ambient temperatures. While both chemistries can extend their cycle life by restricting the depth of discharge (DoD), discharge rate, and controlling temperature, lead acid batteries typically demonstrate greater sensitivity to these factors [103].

c) Rate Performance

When sizing a battery system, a key factor to consider for lead acid batteries is the discharge duration. The available capacity decreases as the discharge period becomes shorter. For instance, a 100 Amp hour valve-regulated lead acid (VRLA) battery may only deliver 80 Amp hours if discharged over four hours. On the other hand, lithium-ion battery systems demonstrate superior capacity retention even under high discharge rates. A 100 Amp hours lithium-ion system can achieve over 98 Amp hours of capacity, even with a rapid 30 minute discharge [104].

d) Cold Weather Performance

While both lead acid and lithium-ion battery technologies experience capacity degradation in cold weather conditions, lithium-ion batteries tend to demonstrate superior capacity retention, especially at extremely low temperatures around -20°C (-4°F) and below. The capacity loss for lithium-ion batteries is significantly less pronounced than that of lead acid batteries when operating in such frigid environments [104]. The rate at which a lead acid battery is discharged has a noticeable effect on its output capacity. Consequently, two distinct values for the rated capacity of a Valve Regulated Lead Acid (VRLA) battery may be specified, reflecting the impact of different discharge rates.

e) Environmental Impact

From an environmental perspective, lithium-ion batteries have a clear advantage over lead acid batteries. To achieve the same energy storage capacity, lead acid technology requires several times more raw material mining than lithium-ion, resulting in a significantly larger environmental impact during the resource extraction phase.

Moreover, the lead manufacturing industry is highly energy intensive, contributing to substantial pollution and contamination levels. Although lead poses serious health hazards to humans, the manufacturing processes and battery packaging generally mitigate direct exposure risks to negligible levels.

However, lead acid batteries do offer one notable environmental benefit - their high recycling rate. In the United States, over 97% of used lead acid batteries are recycled, positively impacting their overall environmental footprint. This high recycling rate helps minimize the need for new raw material mining while preventing lead contamination in the environment from improperly disposed batteries. Effective recycling programs are crucial for reducing the ecological impact of lead acid battery technology [105].

It's important to recognize that lithium-ion batteries also pose environmental challenges [105]. While lithium is a key component, these batteries rely on several other essential raw materials like lithium carbonate, copper, aluminum, and iron ore. The environmental impact stems not just from lithium mining, but also from the resource intensive processes required to obtain the larger quantities of aluminum and copper used in the battery cells.

Currently, the lithium-ion battery recycling industry is still in its infancy. However, the materials used in lithium-ion cells have a high potential for recovery and recyclability. As recycling technologies continue to advance, it is anticipated that lithium-ion battery recycling rates will eventually surpass those of lead acid batteries. Increasing lithium-ion battery recycling is crucial for minimizing their environmental footprint and promoting a more sustainable approach to battery production and end of life management.

e) **Safety**

Both lead acid and lithium-ion battery technologies carry the risk of experiencing a phenomenon known as "thermal runaway". This condition occurs when the battery cell rapidly overheats, potentially leading to the release of electrolyte, flames, and hazardous fumes. However, the probability and severity of such an event tend to be higher for lithium-ion batteries due to their higher energy density packed into a smaller volume compared to lead acid cells.

While thermal runaway is a safety concern for both battery chemistries, the consequences of such an incident may be more severe in lithium-ion battery systems. This is primarily due to the

greater concentration of energy within a compact space, which can exacerbate the intensity and potential for propagation of a thermal event if not properly managed through robust safety systems and engineering controls.

Various safety precautions, as depicted in Figure II.9, are implemented for both multiple cell and pack configurations to mitigate the risk of triggering events like short circuits and overheating. Despite these precautions, incidents involving thermal runaway still occur, highlighting the importance of ongoing research and development in battery safety technology [106].

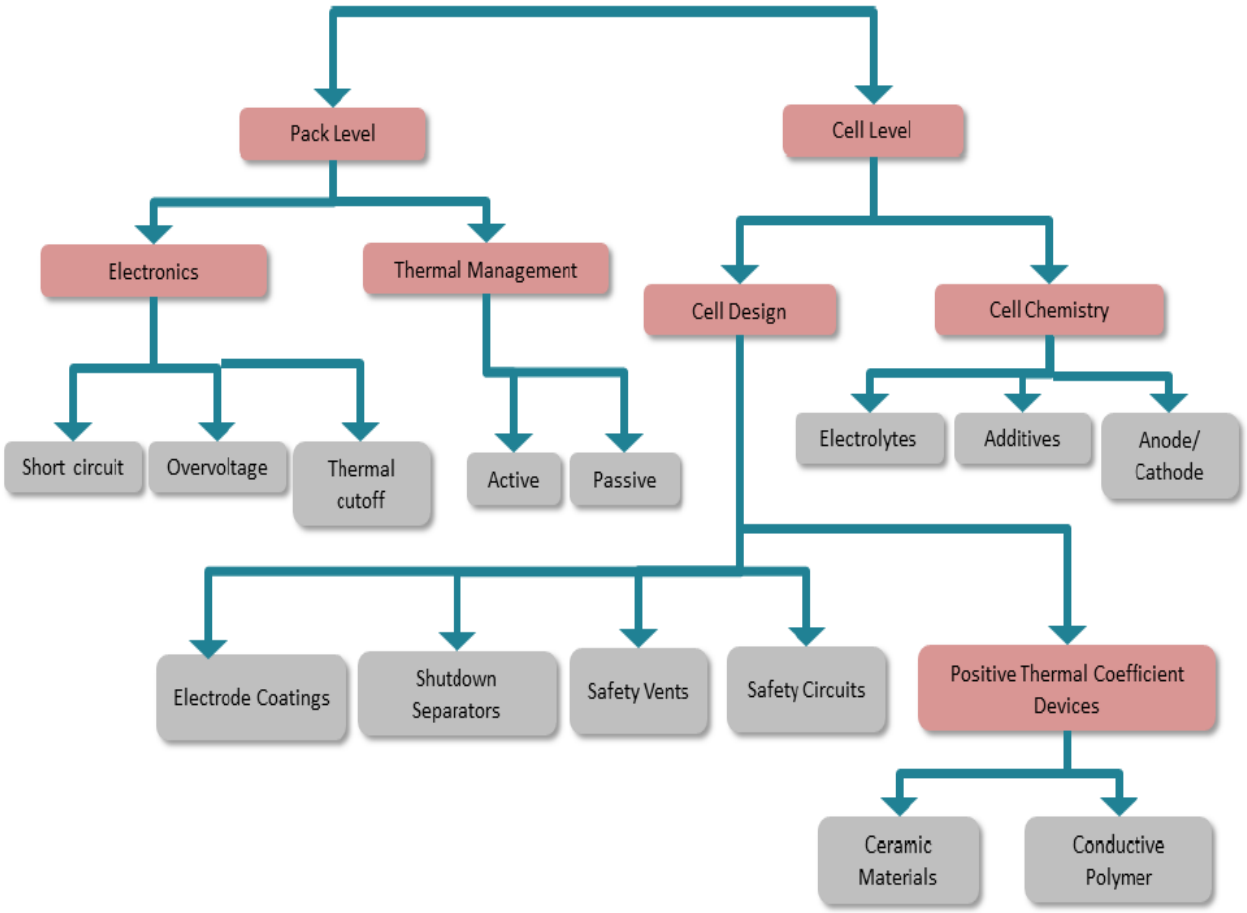

Figure II.9: *Lithium-ion Safety Mechanisms [106].*

f) **Voltage Comparaison**

The primary consideration for determining whether lithium-ion and lead acid batteries can be swapped in a particular electrical device is their voltage compatibility. While lithium-ion batteries generally align well with lead acid systems across most voltage ranges, any electrical

system must be capable of handling the higher charging voltage required for lithium-ion batteries to achieve optimal performance [107].

Numerous batteries charging controllers and discharge inverters used in renewable energy setups are capable of switching between lead acid and lithium-ion batteries. Manufacturers of charge controllers, inverters, as well as lithium-ion companies, often collaborate to ensure that devices are compliant with both battery types.

II.6 Conclusion:

In this chapter, we learned about the types of batteries, how to charge them, and their most important models. We talked about lithium batteries and lead acid batteries, because they are the most widely used and most efficient. But in the next chapter we will study the lead acid battery because it is available. We will also discuss the study of experimental battery models because they are easy to implement and computationally efficient.

CHAPTER III

Experimental and Simulation Results and Comments

Chapter III: Experimental and simulation results and comments

III.1 Introduction

In this chapter, we will learn about the coulomb counting method and the experimental battery model and how to exploit them to estimate the SOC of lead acid batteries. A comparison will be made between the theoretical and practical results to prove the validity of the method.

III.2 Generic Battery Model

To represent the battery's behavior, a circuit model can be formulated by coupling a constant voltage source consecutively with a fixed resistor. This arrangement leads to a mathematical expression that characterizes the battery's output in terms of its internal parameters [108].

$$V_{batt} = \mathbf{E_0} - \mathbf{K}\frac{Q}{Q-i_t} \cdot i_t - \mathbf{R} \cdot \mathbf{I} + \mathbf{A} \cdot \mathbf{exp}(-\mathbf{B} \cdot i_t)\mathbf{K}\frac{Q}{Q-i_t} \cdot i^* \quad \textbf{(III.1)}$$

A distinguishing characteristic of this model is its use of a filtered current (i*) that flows through the polarization resistance component. Employing this filtered current signal helps circumvent the algebraic loop issues that can arise when simulating power system models within the Simulink environment [109].

While there is a hysteresis effect present, where the battery voltage exhibits differences between the charging and discharging phases, this model can be applied to accurately represent the battery's behavior during both the charge and discharge cycles [110]. The battery models can be obtained using:

- ✓ The charge model ($i^* < 0$)

$$f_1(it, i^*, \mathbf{exp}, \mathbf{batt\ type}) = \mathbf{E_0} - \mathbf{K}\frac{Q}{i_t - 0.1Q} \cdot i * -\mathbf{K}\frac{Q}{i_t - Q} \cdot i_t + \mathbf{Exp}\ (t) \quad \textbf{(III.2)}$$

- ✓ The dicharge model ($i^* > 0$)

$$f_1(it, i^*, \mathbf{exp}, \mathbf{batt\ type}) = \mathbf{E_0} - \mathbf{K}\frac{Q}{i_t - Q} \cdot i * -\mathbf{K}\frac{Q}{i_t - Q} \cdot i_t + \mathbf{Exp}\ (t) \quad \textbf{(III.3)}$$

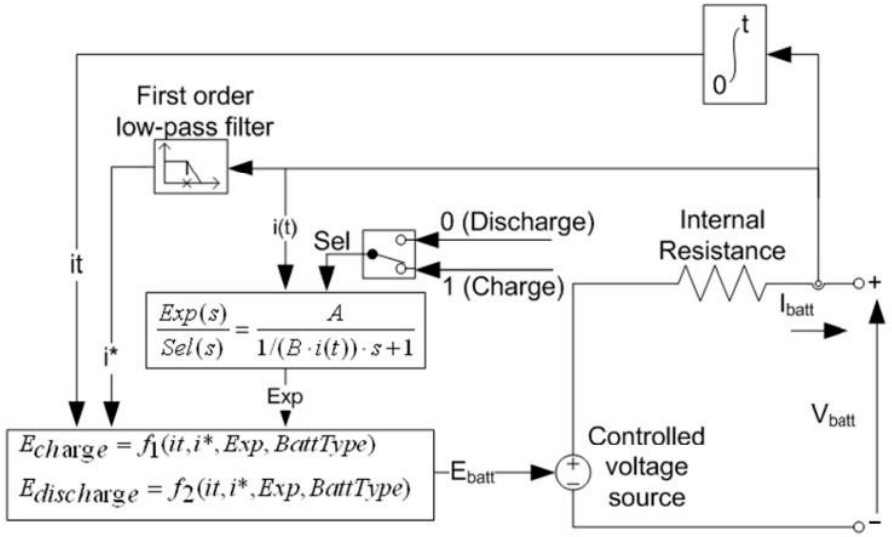

Figure III.1: *A visual representation and characterization of the battery model utilized in this study.*

III.3 Coulomb Counting Method

In this work, the coulomb counting technique (also referred to as the current integration method) is chosen as the baseline approach, as it remains one of the most prevalent and widely adopted methods for state of charge (SOC) estimation [111]. The coulomb counting procedure begins by measuring the battery's open circuit voltage when the system is first initiated, utilizing data from the battery manufacturer's datasheet to estimate the initial SOC level. Following this, the battery's current measurements are integrated over time to calculate the total charge that has been supplied from or replenished to the battery cells. The overarching concept is illustrated in the following manner Equation (III.4), Whereas having knowledge of the initial SOC is crucial for accurately determining the state of charge [112-114]. Following this approach, the State of Charge (SOC) for the battery pack is calculated as follows [115]:

$$\mathbf{SOC} = \mathbf{SOC_0} - \frac{\mathbf{1}}{\boldsymbol{C_N}} \int_{\boldsymbol{t0}}^{\boldsymbol{t}} \boldsymbol{\eta} \cdot \boldsymbol{I}(\boldsymbol{\tau}) \boldsymbol{d\tau} \qquad \textbf{(III.4)}$$

The coulomb counting method provides precise state of charge (SOC) estimation in a relatively straightforward and simple manner when the initial SOC value is specified or known in advance. Typically, researchers will set the initial condition to either a fully charged or fully discharged state [116]. However, the accuracy of this method suffers when the starting SOC is unknown.

The fundamental principle behind the coulomb counting strategy is to calculate the remaining energy stored in the battery by tracking the charge flow into and out of the battery over time. The accuracy hinges on two key factors obtaining accurate battery current measurements and correctly determining the initial SOC value. With prior knowledge of the initial SOC, which can be stored in flash memory at the end of a vehicle trip and then reused as the starting SOC for the next trip (while accounting for any self discharge), the battery's SOC can be estimated by analyzing the total charging and discharging energy flows during operation. However, not all of the stored battery energy is usable due to the depth of discharge (DOD) limit, which reserves a portion of the energy inside to prevent permanent damage. Losses during the charging and discharging processes also impact the total usable capacity. To enable precise SOC assessment, these depth of discharge effects and cycling losses must be accounted for [117].

Furthermore, the SOC estimation requires consistent recalibration, and the discharge limit threshold must be considered to obtain a precise assessment

III.4 Application

According to the discharge data provided by the manufacturer, the extracted battery model parameters are presented in Table III.1 and Table III.2. However, it's important to note that this model has certain inherent assumptions and Limitations:

a) <u>Limitations :</u>

- The battery voltage cannot fall below 0V or exceed twice the nominal voltage (2 x E0).
- The battery capacity must remain within the range of 0Ah to the specified maximum capacity (Qmax).

b) <u>Assumption :</u>

- The internal resistance value is treated as constant, not varying with charge/discharge current.
- The parameter values are derived from discharge curves but assumed to be equally applicable during charging.
- Battery capacity is considered independent of discharge current rate (no Peukert effect).
- The model does not account for temperature effects on performance.

- Self-discharge behavior is not modeled, though it could be approximated by a parallel resistance.
- The battery is assumed to have no memory effects from past usage.

Table III.1: Battery parameters:dicharge at 0.6C.

C-Rates of Discharge	**0.6C**
Nominal voltage (V)	12
Rated capacity (Ah)	7
Initial state of charge (%)	100
Max. capacity (Ah)	4.41
Fully Charged voltage (V)	12.96
Nominal discharge current (A)	4.2
Nominal discharge (**Ω**)	0.0205
Capacity (Ah) @nominal	1.925
Exp. Zone [Voltage (V), capacity (Ah)]	[12.37,0.07]

Table III.2: Battery parameters:dicharge at 1C.

C-Rates of Discharge	**1C**
Nominal voltage (V)	12
Rated capacity (Ah)	7
Initial state of charge (%)	100
Max. capacity (Ah)	4.025
Fully Charged voltage (V)	12.94
Nominal discharge current (A)	7
Nominal discharge (**Ω**)	0.0205
Capacity (Ah) @nominal	0.7
Exp. Zone [Voltage (V), capacity (Ah)]	[12.17,0.116]

III.5 Experimental Method and Description

a) Battery Specification:

In this work, we used a lead acid battery whose characteristics are as follows:

$V_0 = 12\ \mathrm{V}$

$C_n = 7$ Ah

$U = 2.3$ V/Cell

Table III.3 shows the most important features of the battery we used

Table III.3: Specification in our battery Model.

Volts	**12V**	
Capacity (25°C)	20 hours rate (0.35A)	7 Ah
Discharge Current Testing (25°C)	20 I_{20} rate (7A, 27min)	36 min
	60 I_{20} rate (7A, 07min)	8 min
Internal Resistance	Full Charged Battery 25°C	20.5 m
Capacity Affected By Temperature	40°C	104%
	25 °C	100%
	0°C	83%
	-15°C	65%
Residual Capacity (25°C)	Capacity After 3 Months Storage	91%
	Capacity After 6 Months Storage	82%
	Capacity After 12 Months Storage	65%
Charge (Constant Voltage)	Cycle (25°C)	Initial Charging Current Less Than 2.1A Voltage 14.5~14.9V
	Float (25°C)	Charge Voltage 13.6~13.8V
Weight (Approx)		2.09Kg

b) Measurement test bench:

Figure III.2 represents the experimental setup for evaluation and testing:

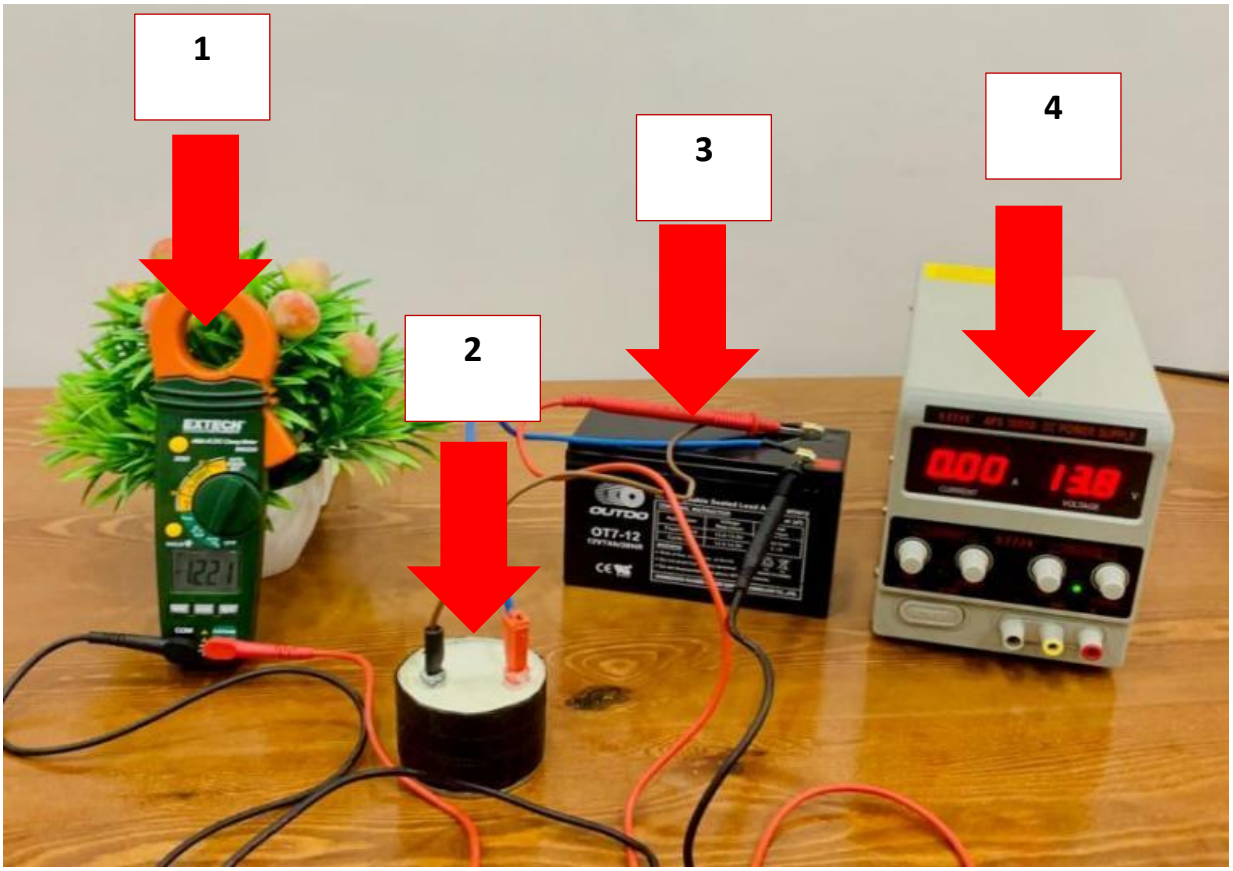

***Figure III.2**: Test Bench.*

1.Clamp Meter

2. A Variable Resistor (Handmade)

3..A Lead Acid Battery

4.DC Power Supply

c) Charging process test:

Using an external DC power source, the battery is charged, and its characteristics are set as follows:

V_0= 13.8 V, I_{max}=1.4 A

Action Steps:

- We charge the battery with the power source until it is full

- We measure the voltage and current every 10 minutes using a voltmeter and a clamp meter

- After the end of charging, we find the following results:

Vfinish-ocv= 13.82 V

Imin= 0.02A.

- After the current value stabilizes at 0.02 A, we stop the charging process that took place within 22 hours and thus:

Tch = 1320 min or Tch = 22 h.

d) Discharging process test:

- Discharging with constant C-rates:

In order to discharge the battery, we connected it to a variable resistor (to adapt to the variable C equations). We conduct statistics every 5 minutes to measure the voltage and discharge current using a clamp measuring device.

For 1 C, after 32 minutes, the discharge voltage reaches its last limit, which is 9.5 V. And for 0.6 C, after 60 minutes, the discharge voltage reaches its last limit, which is 9.7 V.

Next, we stop the discharge process by disconnecting the battery and the discharge resistor from each other.

For 1 C:

Rdisch = [1.7–1.8] Ω

T = 25.9 ◦C

For 0.6:

Rdisch = [2.85–2.95] Ω

T =26.2 ◦C

III.6 Results and Discussion

Through Figure III.3 ,the voltage readings illustrate an electrochemical depletion pattern during the 0.6C discharge cycle. As the chronological markers progress, the reduced potential aligns with a predetermined threshold of 9.7V after the 60 minute interval has elapsed. This defined limit serves as a precautionary barrier to circumvent adverse effects on the storage medium. However, the numerical value does not symbolize an absolute evacuation of electrochemical reserves. Instead, it denotes a conditional benchmark correlating to the retention of approximately one fifth of the total energetic capacity (soc value in the vicinity of 20%). Operating beyond this calibrated reference point could potentially inflict permanent impairment on the device's functional integrity [118].

The trajectory of the empirical drainage sequence exhibits a notable parallel to the artificially constructed projection, apart from distortions attributable to sensory fluctuations and deviations within the collated data points. This discrepancy implies that the storage device's energetic output is susceptible to variations contingent upon the prevailing operational parameters and user-defined configurations, such as the recharging protocol, ambient thermal conditions, and the magnitude of the discharge current flow. It is prudent to acknowledge that the manufacturer supplied specifications typically align with an idealized scenario characterized by a standardized temperature of 25◦C Celsius, a discharge current intensity of 4.2 A, and an assumption of pristine operational status (SOH = 100%), thereby representing the performance characteristics of a newly manufactured unit. Consequently, the experimental findings reveal a significant degree of congruence among the three data sets the manufacturer's datasheet, the simulated model, and the empirical observations which serves as an indication that the battery model employed in this study exhibits a highly precise capacity to emulate the discharge phase of the storage device.

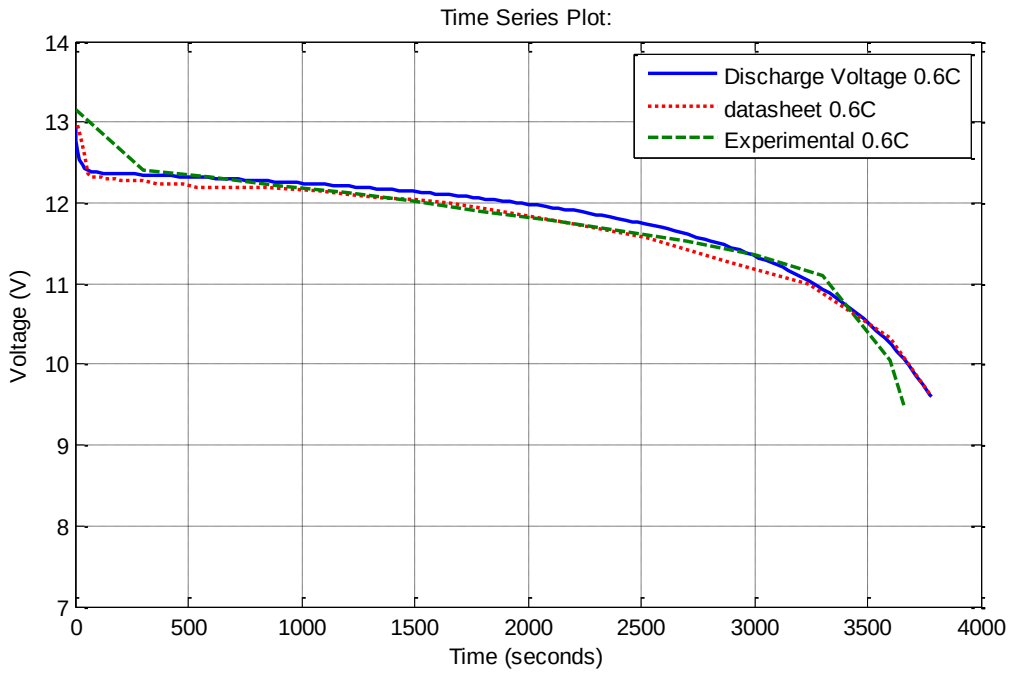

Figure III.3. *Discharge voltage 0.6C versus time.*

Through Figure III.4 ,the voltage readings illustrate an electrochemical depletion pattern during the 1C discharge cycle. As the chronological markers progress, the reduced potential aligns with a predetermined threshold of 9.5V after the 32 minute interval has elapsed. This defined limit serves as a precautionary barrier to circumvent adverse effects on the storage medium. However, the numerical value does not symbolize an absolute evacuation of electrochemical reserves. Instead, it denotes a conditional benchmark correlating to the retention of approximately one fifth of the total energetic capacity (soc value in the vicinity of 20%). Operating beyond this calibrated reference point could potentially inflict permanent impairment on the device's functional integrity [118].

The trajectory of the empirical drainage sequence exhibits a notable parallel to the artificially constructed projection, apart from distortions attributable to sensory fluctuations and deviations within the collated data points. This discrepancy implies that the storage device's energetic output is susceptible to variations contingent upon the prevailing operational parameters and user defined configurations, such as the recharging protocol, ambient thermal conditions, and the magnitude of the discharge current flow. It is prudent to acknowledge that the manufacturer supplied specifications typically align with an idealized scenario characterized by a standardized temperature of 25◦C Celsius, a discharge current intensity of 7 A, and an assumption of pristine

operational status (SOH = 100%), thereby representing the performance characteristics of a newly manufactured unit. Consequently, the experimental findings reveal a significant degree of congruence among the three data sets the manufacturer's datasheet, the simulated model, and the empirical observations which serves as an indication that the battery model employed in this study exhibits a highly precise capacity to emulate the discharge phase of the storage device.

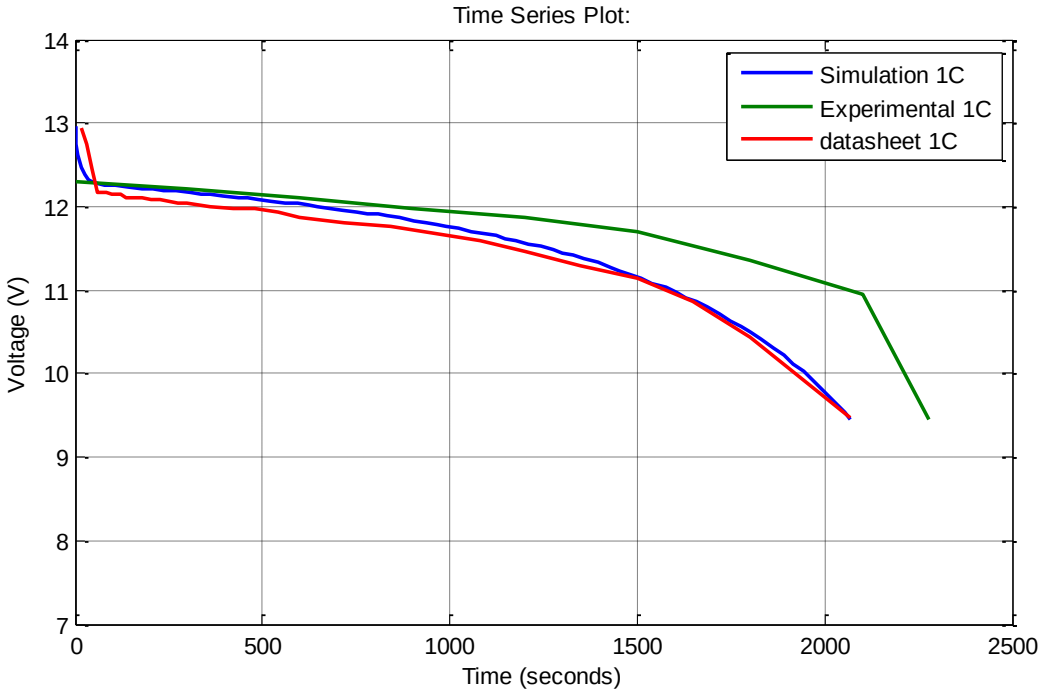

Figure III.4. *Discharge voltage.1C versus time.*

The figure III.5 showcases the estimated state of charge (SOC) behavior as the battery undergoes discharging at fixed C-rates. It can be seen that the battery begins in a fully charged condition (SOC0 = 100%), and the SOC decreases to a minimum threshold value (SOCmin = 20%) after 60 minutes of discharge.

Going below this 20% SOC level must be avoided to prevent causing irreversible damage to the battery, as highlighted for hybrid electric vehicle applications [119].

The straight line represents the SOC curve obtained through the coulomb counting estimation method, where the battery is discharged at a constant current rate (Idisch = 4.2A). This coulomb counting approach enables tracking the battery's SOC evolution across the entire 60 minute discharge cycle.

The results across all the tests clearly demonstrate that the experimentally obtained state of charge values closely align with the simulated SOC calculations. This similarity indicates that the coulomb counting technique exhibits a high degree of accuracy and practical utility due to the straightforward nature of its implementation and the simplicity of the required computations. Moreover, this method is convenient to apply, as it solely relies on the data acquired from current and voltage sensor measurements.

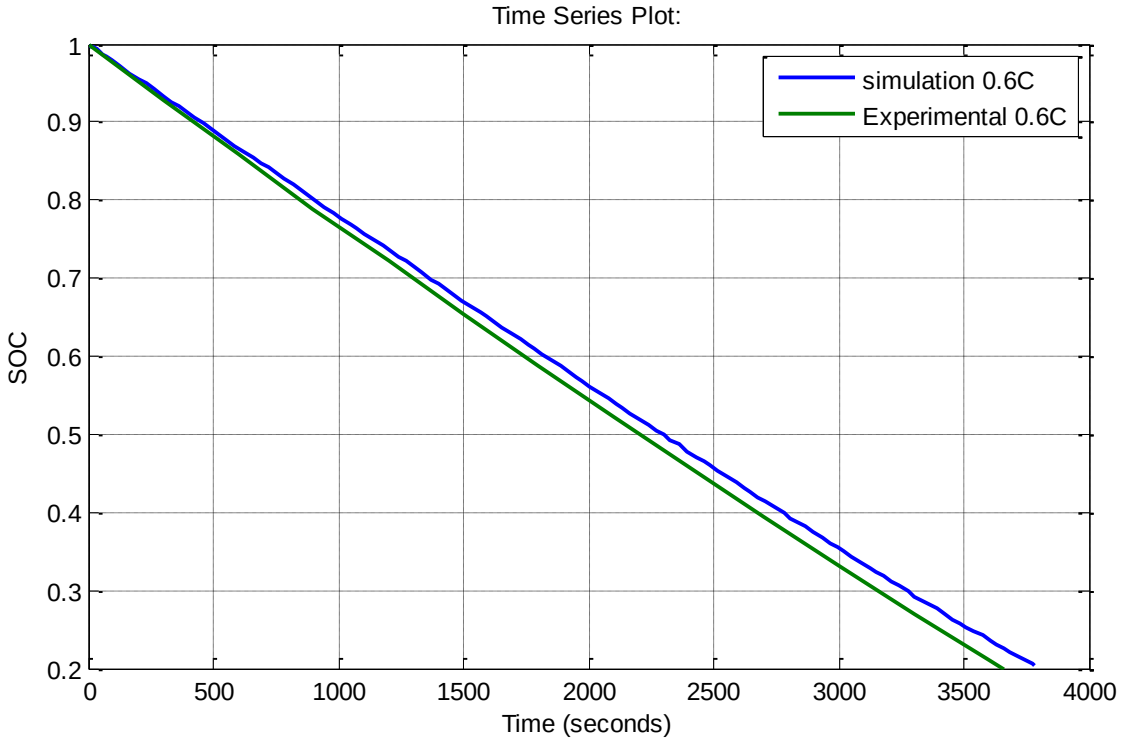

Figure.III.5:. *Discharge SOC 0.6C versus time*

The figure III.6 showcases the estimated state of charge (SOC) behavior as the battery undergoes dicharging at fixed C-rates. It can be seen that the battery begins in a fully charged condition (SOC0 = 100%), and the SOC decreases to a minimum threshold value (SOCmin = 20%) after 32 minutes of discharge.

Going below this 20% SOC level must be avoided to prevent causing irreversible damage to the battery, as highlighted for hybrid electric vehicle applications [119].

The straight line represents the SOC curve obtained through the coulomb counting estimation method, where the battery is discharged at a constant current rate (Idisch = 7A). This coulomb

counting approach enables tracking the battery's SOC evolution across the entire 32 minute discharge cycle.

The results across all the tests clearly demonstrate that the experimentally obtained state of charge values closely align with the simulated SOC calculations. This similarity indicates that the coulomb counting technique exhibits a high degree of accuracy and practical utility due to the straightforward nature of its implementation and the simplicity of the required computations. Moreover, this method is convenient to apply, as it solely relies on the data acquired from current and voltage sensor measurements.

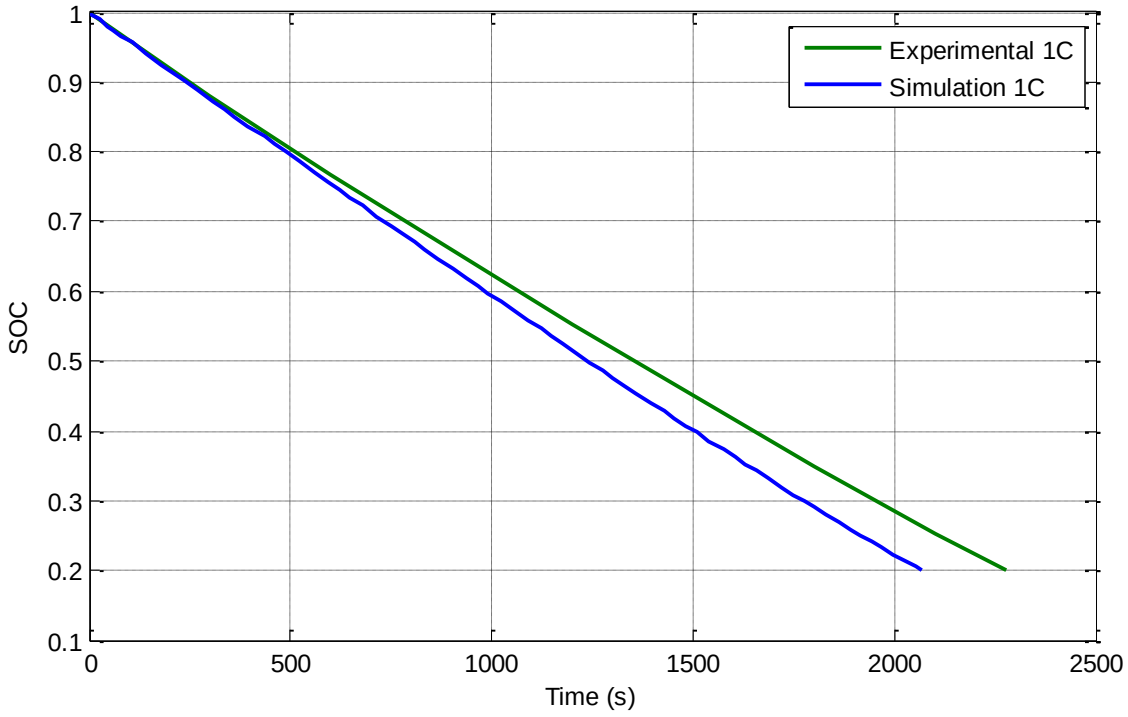

Figure.III.6: *Discharge SOC 1C versus time.*

The graphical representation denoted as Figure III.7 elucidates the initial voltage state of the electrochemical storage device, which is calibrated to 12.6V for both the empirical and manufacturer provided data plots. Furthermore, the commencing charge condition is quantified as SOC0 = 20% [115].

Upon examination, it can be discerned that the voltage parameter undergoes a rapid ascension, attaining a value of approximately 13.8V, whereupon it maintains a steady state. Two distinct regimes are observable the first being a mode characterized by a constant current [116], spanning

a temporal duration of 1.25×10^4 seconds for the datasheet curve and 0.7×10^4 seconds for the experimental curve.

The second distinguishable regime constitutes a mode governed by a constant voltage, persisting for a period ranging from $(1.25 \text{ to } 7.92)\times10^4$ seconds.

The sole discrepancy between the two curves (experimental and datasheet) manifests in the region corresponding to the constant current charging mode, wherein the durational span of this phase exhibits a disparity, with the datasheet indicating 1.25×10^4 seconds and the experimental data suggesting 0.7×10^4 seconds. Ultimately, the charging phase is contingent upon numerous factors, such as the charging mode, initial SOC, and ambient temperature. This culminates in a total charge period of 22 hours, at which juncture the end-of-charge current attains a value of 0.02A, prompting the deactivation of the DC power supply to circumvent overcharging.

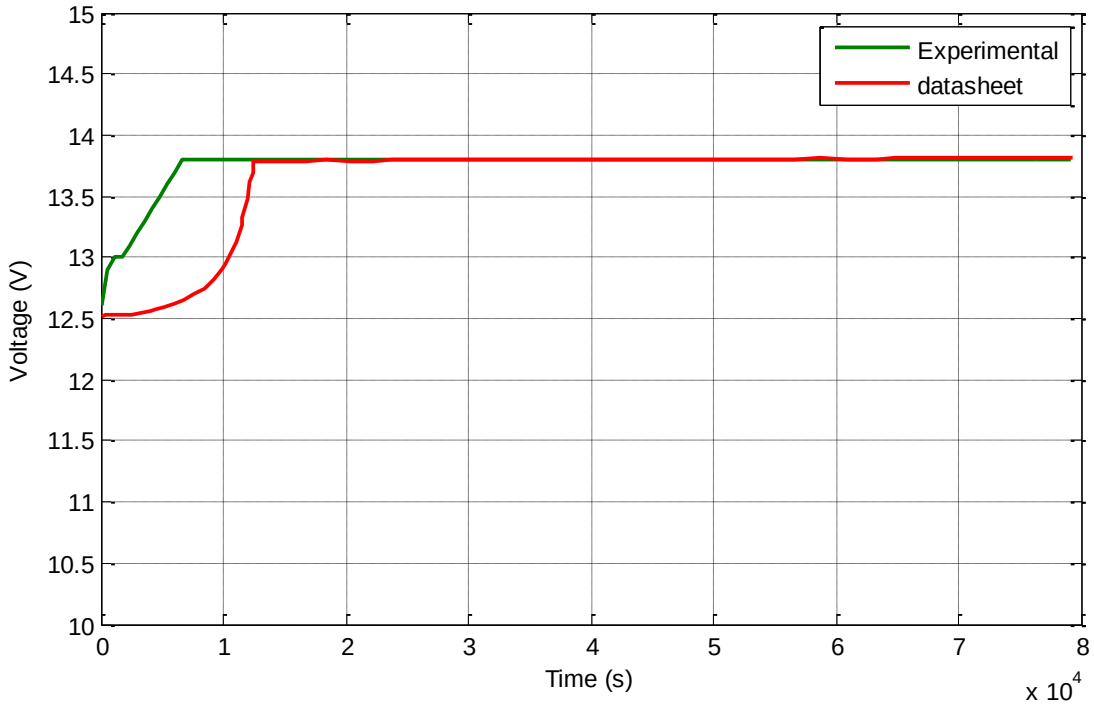

Figure.III.7: *charge voltage versus time.*

The graphical representation identified as Figure III.8 elucidates that the initial quantification of the charge state, denoted as SOC0, is established at 20% when the temporal parameter t assumes a value of zero.

Consequently, this charge state undergoes an incremental progression, conforming to the charging relation, until it attains a magnitude of 100%, thereby signifying a state of complete charge saturation within the electrochemical storage device.

The curvilinear trajectory can be segregated into two distinct segments. The first segment, spanning a temporal duration from (0 to 1.8)×10^4 seconds on the temporal scale, corresponds to a mode characterized by a constant current charging regime. This segment exhibits a nearly linear configuration, typified by a rapid temporal variation in the charge state parameter. For instance, at the 1.8×10^4 seconds, the experimentally obtained charge state assumes a value of approximately 60%, while the charge state derived from the datasheet is quantified as 80%.

The second segment manifests as a nonlinear curvilinear configuration, representing a charging mode governed by a constant voltage regime. This segment is distinguished by a relatively diminished rate of variation in the charge state parameter. As an illustrative example, during the temporal interval spanning from (1.8 to 7.92)×10^4 seconds, the experimentally obtained charge state undergoes an incremental increase of 40%, while the charge state derived from the datasheet exhibits an increase of 20%.

Consequently, it can be deduced that the charge storage capacity of the electrochemical device is contingent upon the charging mode employed, with the constant current mode facilitating a more expeditious charge rate compared to the constant voltage mode. This characteristic serves as the rationale for the development of newer charging systems that prioritize expedited charging durations, particularly for lead acid battery technologies.

Moreover, Figure III.8 demonstrates that the coulomb counting approach furnishes a fair and accurate depiction of the charge state throughout the entirety of the charging process.

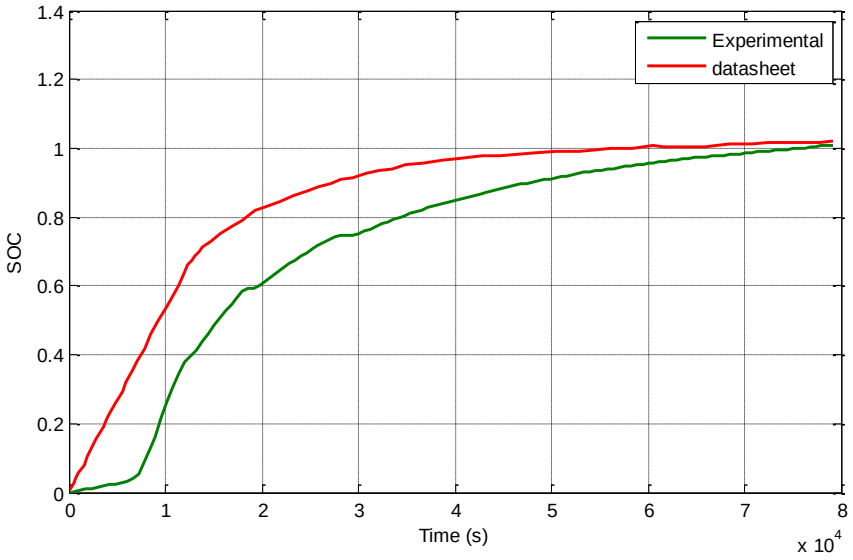

Figure.III.8: *charge SOC versus time.*

III.7 Realisation of state of charge board

For my final project, I am developing a device using Arduino technology to estimate the State of Charge of batteries. This project is driven by the need for affordable, accessible, and practical battery monitoring solutions suitable for various applications, ranging from small scale electronics to renewable energy systems.

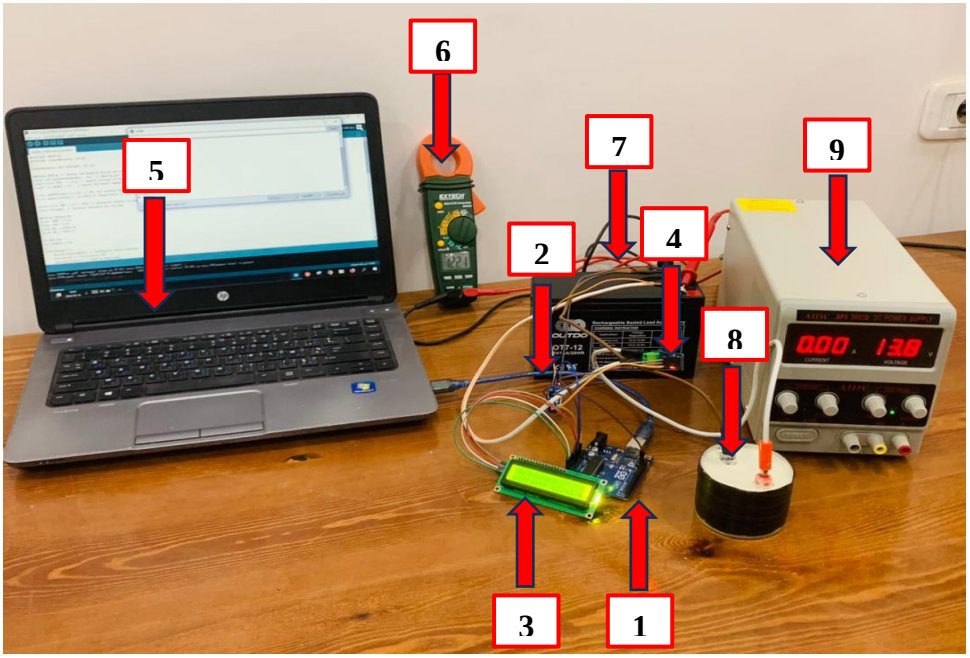

Figure III.09*: Test Bench*

Components Required:

1.Arduino board (e.g., Arduino Uno)

2. ACS712 current sensor module

3.16x2 I2C LCD display

4.Sensor voltage:

5.PC

6. Clamp Meter

7 A Lead Acid Battery

8 A Variable Resistor (Handmade)

9. DC Power Supply

III.7.1 Wiring Instructions:

- **Connect ACS712 Current Sensor:**
  - VIN (VCC): Connect to Arduino 5V.
  - GND: Connect to Arduino GND.
  - OUT: Connect to Arduino analog input pin A1 (defined as VIN in the sketch).
- **Set Up Voltage Divider for Voltage Measurement:**
  - Connect R1 (30k ohms) between Sensor (A0) and ground (GND).
  - Connect R2 (7.5k ohms) between Sensor (A0) and Arduino 5V (VCC).
  - The point between R1 and R2 connects to Sensor (A0).
- **LCD Display (I2C Connection):**
  - GND: Connect to Arduino GND.
  - VCC: Connect to Arduino 5V.
  - SDA: Connect to Arduino A4 (for Uno) or SDA pin (for other Arduino models).
  - SCL: Connect to Arduino A5 (for Uno) or SCL pin (for other Arduino models).
  - Backlight (if available): Connect to Arduino 5V and GND for backlight control.

III.7.2 Working sketchs in the Arduino program

```
#include <Wire.h>
#include <LiquidCrystal_I2C.h>

LiquidCrystal_I2C lcd(0x27, 16, 2); // set the LCD address to 0x27 for a 16 chars and 2 line display

void setup()
{
  lcd.init();         // initialize the lcd
  lcd.backlight();    // Turn on the LCD screen backlight
}

void loop()
{
  lcd.setCursor(1, 0);
  lcd.print("Hello World.!");
  delay(3000);
  lcd.clear();

  lcd.setCursor(2, 0);
  lcd.print("This is a LCD ");
  lcd.setCursor(2, 1);
  lcd.print("Screen Test");
  delay(3000);
  lcd.clear();
}
```

***Figure III.10**: Sketch I2C_LCD.*

```
#include <LiquidCrystal_I2C.h>
LiquidCrystal_I2C lcd(0x27, 16, 2);

#define Sensor A0
float vOUT = 0.0;
float vIN = 0.0;
float R1 = 30000.0;
float R2 = 7500.0;

void setup() {
  Serial.begin(9600);
  lcd.init();
  lcd.backlight();
}

void loop() {
  int value = analogRead(Sensor);
  vOUT = (value * 5.0) / 1024.0;
  vIN = vOUT / (R2 / (R1 + R2));

  lcd.setCursor(0, 0);
  lcd.print("Voltage :");
  lcd.print(vIN);
  lcd.print("v ");
  Serial.print("Voltage : ");
  Serial.println(vIN);
  delay(1000);
}
```

***Figure III.11**: Diagrammatic representation that depicts the operational principle of a voltage measurement device.*

```
#define VIN A1 // define the Arduino pin A0 as voltage input (V in)
const int currentSensorPin = A1;  // Analog pin connected to ACS712 current sensor
const float VCC   = 5.0;// supply voltage is from 4.5 to 5.5V. Normally 5V.
const int model = 0;   // enter the model number (see below)

float cutOffLimit = 1.01;// set the current which below that value, doesn't matter. Or set 0.5

/*
          "ACS712ELCTR-05B-T",// for model use 0
          "ACS712ELCTR-20A-T",// for model use 1
          "ACS712ELCTR-30A-T"// for model use 2
sensitivity array is holding the sensitivy of the  ACS712
current sensors. Do not change. All values are from page 5  of data sheet
*/
float sensitivity[] ={

        0.328  //  0.185     for ACS712ELCTR-30A-T

        };


const float QOV =   0.5 * VCC;// set quiescent Output voltage of 0.5V
float voltage;// internal variable for voltage


// start of settings for LCD1602 with I2C
#include <Wire.h>
#include <LiquidCrystal_I2C.h>
// Set the LCD address to 0x27 for a 16 chars and 2 line display
LiquidCrystal_I2C lcd(0x27, 16, 2);
// end of settings for LCD1602 with I2C

void setup() {
   //Robojax.com ACS712 Current Sensor
   Serial.begin(9600);// initialize serial monitor
   Serial.println("Robojax Tutorial");
   Serial.println("ACS712 Current Sensor");
  // initialize the LCD
  lcd.begin(16, 2);
  lcd.init();         // initialize the lcd

  lcd.backlight();
  lcd.print("Robojax ACS712");
  lcd.setCursor(0,1);
  lcd.print("Demo");
  delay(2000);
}

void loop() {


  //Robojax.com ACS712 Current Sensor with LCD1601
  float voltage_raw =   (5.0 / 1023.0)* analogRead(VIN);// Read the voltage from sensor
  voltage =  voltage_raw - QOV;// 0.000 is a value to make voltage zero when there is no current
  float current = voltage / sensitivity[model];

  if(abs(current) > cutOffLimit ){
    Serial.print("V: ");
    Serial.print(voltage,3);// print voltage with 3 decimal places
    Serial.print("V, I: ");
    Serial.print(current,2); // print the current with 2 decimal places
    Serial.println("A");
    //start of loop Robojax code ACS712 with LCD1602 and I2C
    lcd.clear();
    lcd.setCursor (0,0); // set to line 1, char 0
    lcd.print("Robojax ACS712");
    lcd.setCursor (0,1); // set to line 1, char 0
    lcd.print("Current: ");
    lcd.setCursor (9,1); // go to start of 2nd line
    lcd.print(current);
    lcd.setCursor (14,1); // go to start of 2nd line
    lcd.print("A");

  }else{
    Serial.println("No Current");
    lcd.clear();
    lcd.setCursor (0,0); // set to line 1, char 0
    lcd.print("NO Current");
  }
  delay(2000);
}
```

***Figure III.12**: Diagrammatic representation of a device designed to measure and monitor the flow of electrical current.*

```ino
#include <Wire.h>
#include <LiquidCrystal_I2C.h>

LiquidCrystal_I2C lcd(0x27, 16, 2);

#define VIN A1 // define the Arduino pin A1 as voltage input (V in) for ACS712 current sensor
const int currentSensorPin = A1;  // Analog pin connected to ACS712 current sensor
const float VCC   = 5.0; // Supply voltage is from 4.5 to 5.5V. Normally 5V.
const int model = 0;   // Enter the model number (0 for "ACS712ELCTR-05B-T")

float cutOffLimit = 1.01; // Set the current threshold (in amps) below which "No Current" is displayed
float sensitivity[] = {0.328}; // Sensitivity of the ACS712 current sensor

const float QOV = 0.5 * VCC; // Quiescent Output voltage of 0.5V
float voltage; // Internal variable for voltage

#define Sensor A0
float vOUT = 0.0;
float vIN = 0.0;
float R1 = 30000.0;
float R2 = 7500.0;

// LED Pin
int ledPin = 13;

void setup() {
    Serial.begin(9600); // Initialize serial monitor
    lcd.init(); // Initialize LCD
    lcd.backlight(); // Turn on backlight

    pinMode(ledPin, OUTPUT); // Initialize LED pin
}

void loop() {
    // Read voltage from ACS712 sensor
    float voltage_raw = (5.0 / 1023.0) * analogRead(VIN);
    voltage = voltage_raw - QOV;
    float current = voltage / sensitivity[model];

    // Read voltage using voltage divider
    int value = analogRead(Sensor);
    vOUT = (value * 5.0) / 1024.0;
    vIN = vOUT / (R2 / (R1 + R2));

    if (abs(current) > cutOffLimit) {
        // Print current to Serial monitor
        Serial.print("Current: ");
        Serial.print(current, 2); // Print the current with 2 decimal places
        Serial.println(" A");

        // Display current on LCD
        lcd.clear();
        lcd.setCursor(0, 0);
        lcd.print("Current: ");
        lcd.print(current, 2);
        lcd.print(" A");

        // Blink LED
        digitalWrite(ledPin, HIGH);
        delay(500); // LED on time
        digitalWrite(ledPin, LOW);
        delay(500); // LED off time
```

```
    } else {
        Serial.println("No Current");
        lcd.clear();
        lcd.setCursor(0, 0);
        lcd.print("No Current");

        // Turn off LED
        digitalWrite(ledPin, LOW);
    }

    // Display voltage on LCD
    lcd.setCursor(0, 1);
    lcd.print("Voltage: ");
    lcd.print(vIN, 2);
    lcd.print(" V");

    // Print voltage to Serial monitor
    Serial.print("Voltage: ");
    Serial.print(vIN, 2);
    Serial.println(" V");

    delay(1000); // Delay between readings
}
```

***Figure III.13**: Sketch Combination.*

```
#include <Wire.h>
#include <LiquidCrystal_I2C.h>

LiquidCrystal_I2C lcd(0x27, 16, 2);

#define VIN A1 // define the Arduino pin A1 as voltage input (V in) for ACS712 current sensor
const int currentSensorPin = A1;  // Analog pin connected to ACS712 current sensor
const float VCC   = 5.0; // Supply voltage is from 4.5 to 5.5V. Normally 5V.
const int model = 0;   // Enter the model number (0 for "ACS712ELCTR-05B-T")

float cutOffLimit = 1.01; // Set the current threshold (in amps) below which "No Current" is displayed
float sensitivity[] = {0.118}; // Sensitivity of the ACS712 current sensor

const float QOV = 0.5 * VCC; // Quiescent Output voltage of 0.5V
float voltage; // Internal variable for voltage

#define Sensor A0
float vOUT = 0.0;
float vIN = 0.0;
float R1 = 30000.0;
float R2 = 7500.0;
```

```
22
23  const float batteryCapacity = 7.0; // Battery capacity in Ah (7Ah)
24  float cumulativeCurrent = 0.0; // Cumulative charge in Ah
25  unsigned long previousTime = 0;
26
27  int ledPin = 13;
28
29  void setup() {
30      Serial.begin(9600); // Initialize serial monitor
31      lcd.init(); // Initialize LCD
32      lcd.backlight(); // Turn on backlight
33
34      pinMode(ledPin, OUTPUT); // Initialize LED pin
35
36      previousTime = millis(); // Set initial time
37  }
38
39  void loop() {
40      // Read voltage from ACS712 sensor
41      float voltage_raw = (5.0 / 1023.0) * analogRead(VIN);
42      voltage = voltage_raw - QOV;
43      float current = voltage / sensitivity[model];
44
45      // Read voltage using voltage divider
46      int value = analogRead(Sensor);
47      vOUT = (value * 5.0) / 1024.0;
48      vIN = vOUT / (R2 / (R1 + R2));
49
50      // Calculate elapsed time
51      unsigned long currentTime = millis();
52      float deltaTime = (currentTime - previousTime) / 1000.0; // Convert to seconds
53      previousTime = currentTime;
54
55      // Integrate current over time
56      cumulativeCurrent += current * deltaTime / 3600.0; // Convert to Ah
57
58      // Calculate SoC
59      float soc = 100.0 - (0.98 / batteryCapacity) * cumulativeCurrent * 100.0; // SoC as a percentage
60
61      if (abs(current) > cutOffLimit) {
62          // Print current to Serial monitor
63          Serial.print("I: ");
```

```
        Serial.print(current, 2); // Print the current with 2 decimal places
        Serial.println(" A");

        // Display current on LCD
        lcd.clear();
        lcd.setCursor(0, 0);
        lcd.print("I: ");
        lcd.print(current, 2);
        lcd.print(" A");
    } else {
        Serial.println("No Current");
        lcd.clear();
        lcd.setCursor(0, 0);
        lcd.print("No Current");

        // Turn off LED
        digitalWrite(ledPin, LOW);
    }

    // Display voltage and SoC on LCD
    lcd.setCursor(0, 0);
    lcd.print("U: ");
    lcd.print(vIN, 2);
    lcd.print(" V");

    lcd.setCursor(0, 1);
    lcd.print("SoC: ");
    lcd.print(soc, 2);
    lcd.print(" %");

    // Print voltage and SoC to Serial monitor
    Serial.print("Voltage: ");
    Serial.print(vIN, 2);
    Serial.println(" V");

    Serial.print("SoC: ");
    Serial.print(soc, 2);
    Serial.println(" %");

    delay(1000); // Delay between readings
}
```

***Figure III.14**: Sketch State of Charge.*

III.7.3 Test of SOC power realization

a) Device testing

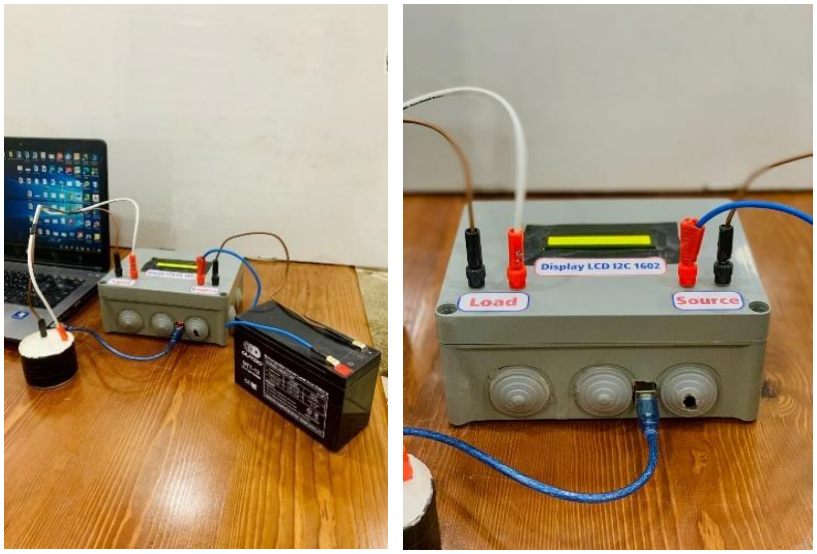

Figure III.15: *Device SOC of measurement*

Figure III.16: *State of charge in initial time*

Figure III.17: *State of charge after 4 min*

Figure III.18: *State of charge after 8 min*

Figure III.19: *State of charge after 12 min*

After creating a device for estimating the state of charge of a lead-acid battery, we conducted an experimental operation within a short time frame. We noticed great convergence and accuracy in the results shown on the device tested and completed using the coulomb counting method.

III.8 Conclusion

A refined Coulomb counting technique is introduced to estimate the State of Charge (SOC) and State of Health (SOH) of lead-acid batteries. The charging and discharging behaviors of lead-acid batteries were meticulously examined. Enhancing estimation precision involved factoring in operational efficiency adjustments and SOH assessments. The investigation yielded several significant conclusions, summarized as follows:

- A battery is classified as fully exhausted and devoid of any remaining power when its voltage drops to a pre-determined critical value. At this very moment, the charging status indicator can be reset to zero, which means that the battery's storage resources are completely depleted.

-The battery can be considered fully depleted once its voltage reaches the cutoff threshold, allowing for the State of Charge (SOC) to be reset to zero at this juncture.

-The battery model employed in SimPowerSystem (MATLAB Simulink) exhibits lower accuracy during charging but demonstrates high precision during discharging, accurately reflecting the battery's behavior during constant current discharge phases.

-The Coulomb counting method utilized for estimating the battery's state of charge proves to be highly accurate.

-The disadvantage of this method lies in its imprecision and the challenge of determining the initial State of Charge (SOC).

General Conclusion

General Conclusion

This thesis focused on the realization of a state of charge (SOC) estimation device for the battery of an electric vehicle (EV). The research was divided into three main chapters: Chapter 1 covered the state of the art of SOC estimation techniques for EV batteries, Chapter 2 detailed various battery models, and Chapter 3 presented experimental and simulation results along with discussions. The study conducted two main tests: online tests with constant and variable discharging current profiles for a real battery pack in a real-time environment.

From the findings of this study, several key conclusions can be drawn:

- Efficiency of Battery Models in Charging Mode: the battery model used in MATLAB Simulink demonstrated less efficiency during charging. However, it remains widely used due to its excellent performance during constant current discharge, making it valuable for comparison purposes despite its shortcomings in the charging mode.
- Coulomb Counting Method: the Coulomb counting method was found to have the significant limitation of difficulty in estimating the initial SOC. High-precision sensors for voltage and current are necessary, and these instruments need regular calibration to maintain accuracy. Despite this, the Coulomb counting method proved useful for SOC estimation, particularly with variable discharge currents.
- Suitability of Lead-Acid Batteries: lead-acid batteries are suitable for short-range vehicles due to their cost-effectiveness. They remain the cheapest form of battery and are practical for small-scale EVs that do not require long-range travel.
- Effectiveness of the proposed SOC estimator: the proposed SOC estimator based on the Coulomb counting technique provided reliable and quick information, which can be integrated into energy management systems. The method showed that constant current discharge, used for fast charging, is effective, and the efficiency of the generic battery model is competitive as its results align closely with experimental data.
- Practical implementation: the proposed method, due to its simplicity in calculations and hardware requirements, can be systematically implemented in portable devices as well as electric cars. The ampere-hour integral method was experimentally validated using a domestic lead-acid battery, demonstrating the method's general applicability.

- Advantages of li-ion batteries: for commercial-scale EVs that require extended travel ranges, modern Li-ion batteries are more suitable. They offer the necessary range and efficiency for such applications.

In conclusion, the research confirmed that the Coulomb Counting method, despite its need for precise initial SOC estimation and high-precision sensors, is a viable approach for SOC estimation. The implementation of this method in future studies for modern Li-ion batteries is recommended, which can further enhance the reliability and efficiency of SOC estimation in EVs. This thesis contributes significantly to the understanding and development of SOC estimation techniques, providing a foundation for future advancements in battery management systems for electric vehicles.

Appendices

Appendices

Appendix: The energy storage device utilized for our research endeavor belongs to the category of OUTDO-**OT7-12**

Figure A.1: *OUTDO-OT7-12 battery picture.*

A. Battery curves

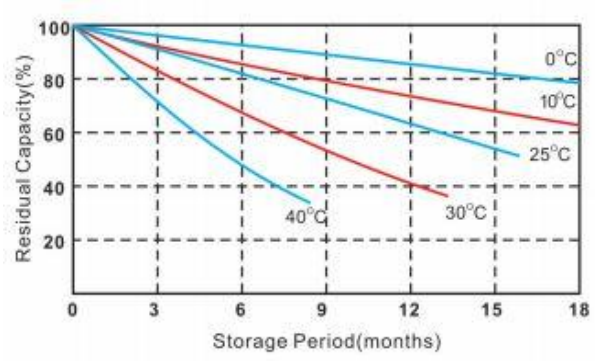

Figure A.2: *The property relating to the ability to maintain charge storage capacity over time.*

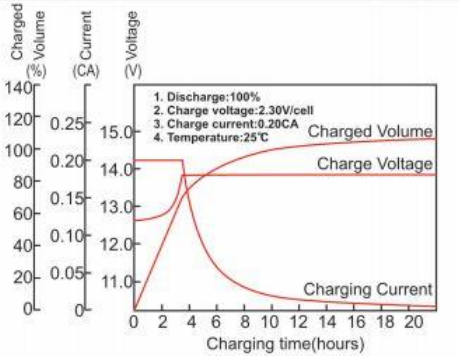

Figure A.3: *Battery Voltage, current and charge capacity versus time.*

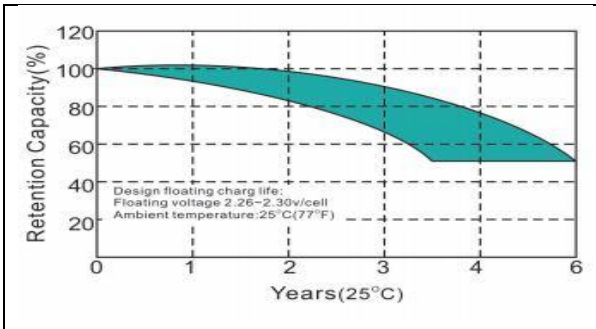

***Figure A.4**: Cycle Service Life*

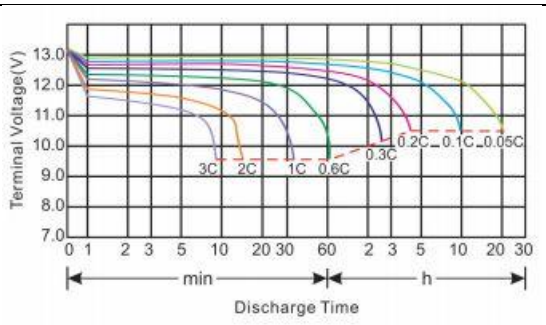

***Figure A.5:** Terminal Voltage (V) and Discharge Time.*

References

References

[1] Zhang, Y.Z.; Xiong, R.; He, H.W.; Pecht, M. Validation and verification of a hybrid method for remaining useful life prediction of lithium-ion batteries. J. Clean. Prod. **2019**, 212, 240–249.

[2] Xiong, R.; Shen, W. Advanced Battery Management Technologies for Electric Vehicles; John Wiley & Sons: Hoboken, NJ, USA, 2019; pp. 1–297.

[3] B. A. Johnson and R. E. White, "Characterization of commercially available lithium-ion batteries," Journal of power sources, vol. 70, no. 1, pp. 48-54, 1998.

[4] J. H. Aylor, A. Thieme, and B. Johnso, "A battery state-of-charge indicator forelectric wheelchairs," IEEE transactions on industrial electronics, vol. 39, no. 5, pp. 398-409, 1992.

[5] Farmann, A.; Waag, W.; Marongiu, A.; Sauer, D.U. Critical review of on-board capacity estimation techniques for lithium-ion batteries in electric and hybrid electric vehicles. J. Power Sources 2015, 281, 114–130.

[6] Hannan, M.A.; Hossain Lipu, M.S.; Hussain, A.; Mohamed, A. A review of lithium-ion battery state of charge estimation and management system in electric vehicle applications: Challenges and recommendations. Renew. Sustain. Energy Rev. 2017, 78, 834–854.

[7] Han, X.; Ouyang, M.; Lu, L.; Jianqiu, L. A comparative study of commercial lithium ion battery cycle life in electric vehicle: Capacity loss estimation. J. Power Sources 2014, 268, 658–669.

[8] Berecibar, M.; Gandiaga, I.; Villarreal, I.; Omar, N.; Van Mierlo, J.; Van den Bossche, P. Critical review of state of health estimation methods of Li-ion batteries for real applications. Renew. Sustain. Energy Rev. 2016, 56, 572–587.

[9] Rahman, M.A.; Anwar, S.; Izadian, A. Electrochemical model parameter identification of a lithium-ion battery using particle swarm optimization method. J. Power Sources 2016, 307, 86–97.

[10] Chang, W.-Y. The State of Charge Estimating Methods for Battery: A Review. ISRN Appl. Math. **2013**, 2013, 953792.

[11] Zhang, C.; Li, K.; Pei, L.; Zhu, C. An integrated approach for real-time model-based state-of-charge estimation of lithium-ion batteries. J. Power Sources **2015**, 283, 24–36.

[12] Lee, J.; Won, J. Enhanced Coulomb Counting Method for SoC and SoH Estimation Based on Coulombic Efficiency. IEEE Access **2023**, 11, 15449–15459.

[13] Espedal, I.B.; Jinasena, A.; Burheim, O.S.; Lamb, J.J. Current Trends for State-of-Charge (SoC) Estimation in Lithium-Ion Battery Electric Vehicles. Energies **2021**, 14, 3284.

[14] G. L. Plett, "Extended Kalman filtering for battery management systems of LiPBbased HEV battery packs: Part 3. State and parameter estimation," Journal of power sources, vol. 134, pp. 277-292, 2004.

[15] G. L. Plett, "Sigma-point Kalman filtering for battery management systems of LiPB based HEV battery packs: Part 2: Simultaneous state and parameter estimation," Journal of power sources, vol. 161, pp. 1369-1384, 2006.

[16] S. Lee, J. Kim, J. Lee, and B. H. Cho, "The state and parameter estimation of an Liion battery using a new OCV-SOC concept," in 2007 IEEE Power Electronics Specialists Conference, 2007, pp. 2799-2803.

[17] R. Van Der Merwe, E. Wan, and S. Julier, "Sigma-point Kalman filters for nonlinear estimation and sensor-fusion: Applications to integrated navigation," in AIAA Guidance, Navigation, and Control Conference and Exhibit, 2004, p. 5120.

[18] F. Yang, Y. Xing, D. Wang, and K.-L. Tsui, "A comparative study of three model based algorithms for estimating state-of-charge of lithium-ion batteries under a new combined dynamic loading profile," Applied energy, vol. 164, pp. 387-399, 2016.

[19] N. Omar, P. Bossche, T. Coosemans, and J. Mierlo, "Peukert revisited—Critical appraisal and need for modification for lithium-ion batteries," energies, vol. 6, pp. 5625-5641, 2013.

[20] J. Meng, G. Luo, and F. Gao, "Lithium polymer battery state-of-charge estimation based on adaptive unscented Kalman filter and support vector machine," IEEE Transactions on Power Electronics, vol. 31, pp. 2226-2238, 2015.

[21] H. He, R. Xiong, X. Zhang, F. Sun, and J. Fan, "State-of-charge estimation of the lithium-ion battery using an adaptive extended Kalman filter based on an improved Thevenin model," IEEE transactions on vehicular technology, vol. 60, pp. 1461- 1469, 2011.

[22] Kim, I.-S. Nonlinear State of Charge Estimator for Hybrid Electric Vehicle Battery. IEEE Trans. Power Electron. **2008**, 23, 2027–2034.

[23] Chen, X.; Shen, W.; Cao, Z.; Kapoor, A.; Hijazin, I. Adaptive gain sliding mode observer for state of charge estimation based on combined battery equivalent circuit model in electric vehicles. Aust. J. Electr. Electron. Eng. **2013**, 9, 601–606.

[24] Boizot, N.; Busvelle, E.; Gauthier, J.-P. An adaptive high-gain observer for nonlinear systems. Automatica **2010**, 46, 1483–1488.

[25] Xu, J.; Mi, C.; Cao, B.; Deng, J.; Chen, Z.; Li, S. The State of Charge Estimation of Lithium-Ion Batteries Based on a ProportionalIntegral Observer. IEEE Trans. Veh. Technol. **2014**, 63, 1614–1621.

[26] Xu, F.; Wang, Y.; Luo, X. Soft Sensor for Inputs and Parameters Using Nonlinear Singular State Observer in Chemical Processes. Chin. J. Chem. Eng. **2013**, 21, 1038–1047.

[27] Kim, I.-S. The novel state of charge estimation method for lithium battery using sliding mode observer. J. Power Sources **2006**, 163, 584–590.

[28] Xia, B.; Chen, C.; Tian, Y.; Sun, W.; Xu, Z.; Zheng, W. A novel method for state of charge estimation of lithium-ion batteries using a nonlinear observer. J. Power Sources **2014**, 270, 359–366.

[29] He, W.; Williard, N.; Chen, C.; Pecht, M. State of charge estimation for Li-ion batteries using neural network modeling and unscented Kalman filter-based error cancellation. Int. J. Electr. Power Energy Syst. **2014**, 62, 783–791.

[30] Chen, Z.; Qiu, S.; Masrur, M.; Murphey, Y.L. Battery state of charge estimation based on a combined model of Extended Kalman Filter and neural networks. In Proceedings of the 2011 International Joint Conference on Neural Networks, San Jose, CA, USA, 31 July–5 August 2011.

[31] Rui-Hao, L.; Yu-Kun, S.; Xiao-Fu, J. Battery state of charge estimation for electric vehicle based on neural network. In Proceedings of the 2011 IEEE 3rd International Conference on Communication Software and Networks, Xi'an, China, 27–29 May 2011.

[32] Salkind, A.J.; Fennie, C.; Singh, P.; Atwater, T.; Reisner, D.E. Determination of state-of charge and state-of-health of batteries by fuzzy logic methodology. J. Power Sources **1999**, 80, 293–300.

[33] Jamlouie, M.H.A. Accuracy improvement of SOC estimation in lithium-ion batteries by ANFIS vs. ANN modeling of nonlinear cell characteristics. J. Energy Storage **2021**, 6, 95–104.

[34] Singh, P.; Vinjamuri, R.; Wang, X.; Reisner, D. Design and implementation of a fuzzy logic-based state-of-charge meter for Li-ion batteries used in portable defibrillators. J. Power Sources **2006**, 162, 829–836.

[35] Malkhandi, S. Fuzzy logic-based learning system and estimation of state-of-charge of lead-acid battery. Eng. Appl. Artif. Intell. **2006**, 19, 479–485.

[36] Li, I.-H.; Wang, W.-Y.; Su, S.-F.; Lee, Y.-S. A Merged Fuzzy Neural Network and Its Applications in Battery State-of-Charge Estimation. IEEE Trans. Energy Convers. **2007**, 22, 697–708.

[37] Cai, C.H.; Du, D.; Liu, Z.Y. Battery state-of-charge (SOC) estimation using adaptive neuro-fuzzy inference system (ANFIS). In Proceedings of the 12th IEEE International Conference on Fuzzy Systems, St. Louis, MO, USA, 25–28 May 2003.

[38] Shen, W.; Chan, C.; Lo, E.; Chau, K.T. Adaptive neuro-fuzzy modeling of battery residual capacity for electric vehicles. IEEE Trans. Ind. Electron. **2002**, 49, 677–684.

[39] Zheng, Y.; Lu, L.; Han, X.; Li, J.; Ouyang, M. LiFePO4 battery pack capacity estimation for electric vehicles based on charging cell voltage curve transformation. J. Power Sources **2013**, 226, 33–41.

[40] Xu, J.; Cao, B.; Chen, Z.; Zou, Z. An online state of charge estimation method with reduced prior battery testing information. Int. J. Electr. Power Energy Syst. **2014**, 63, 178–184.

[41] Antón, J.C.Á.; Nieto, P.J.G.; de Cos Juez, F.J.; Lasheras, F.S.; Vega, M.G.; Gutiérrez, M.N.R. Battery state-of-charge estimator using the SVM technique. Appl. Math. Model. **2013**, 37, 6244–6253.

[42] Wu, X.; Mi, L.; Tan, W.; Qin, J.L.; Na Zhao, M. State of Charge (SOC) Estimation of Ni-MH Battery Based on Least Square Support Vector Machines. Adv. Mater. Res. **2011**, 211–212, 1204–1209.

[43] C. Chen, R. Xiong, W. Shen, A LiB-in-the-loop approach to test and validate multiscale dual H infinity filters for state-of-charge and capacity estimation, IEEE Trans. Power Electron. 1 (33) (2017) 332–342.

[44] M. Lagraoui, S. Doubabi, A. Rachid, SOC estimation of LiB using Kalman filter and Luenberger observer: a comparative study, in: Proceedings of the International Renewable and Sustainable Energy Conference (IRSEC), Ouarzazate, Morocco, 2014, pp. 636–641, 17-19 October.

[45] B. Yang, J.B. Wang, X.S. Zhang, T. Yu, W. Yao, H.C. Shu, F. Zeng, L.M. Sun, Comprehensive overview of meta-heuristic algorithm applications on PV cell parameter identification, Energy Convers. Manag. 208 (2020), 112595.

[46] J. Xu, B. Cao, Z. Chen, Z. Zou, An online state of charge estimation method with reduced prior battery testing information, Int. J. Electr. Power Energy Syst. 63 (2014) 178–184.

[47] C. Lin, X. Zhang, R. Xiong, F. Zhou, A novel approach to state of charge estimation using extended kalman filtering for lithium-ion batteries in electric vehicles, in: Proceedings of the IEEE Transportation Electrification Conference & Expo 2014 (ITEC Asia-Pacific), Beijing, China, 2014, 31 August–3 September.

[48] M.R. Khan, G. Mulder, J. Van Mierlo, An online framework for state of charge determination of battery systems using combined system identification approach, J. Power Sources 246 (2014) 629–641.

[49] L. Chen, Z. Wang, Z. Lü, J. Li, B. Ji, H. Wei, H. Pan, A novel state-of-charge estimation method of lithium-ion batteries combining the grey model and genetic algorithms, IEEE Trans. Power Electron. 33 (2018) 8797–8807.

[50] S. Blaifi, S. Moulahoum, I. Colak, W. Merrouche, An enhanced dynamic model of battery using genetic algorithm suitable for photovoltaic applications, Appl. Energy 169 (2016) 888–898.

[51] H. Mu, R. Xiong, H. Zheng, Y. Chang, Z. Chen, A novel fractional order modelbased state-of-charge estimation method for lithium-ion battery, Appl. Energy 207 (2017) 384–393.

[52] N.K. Jhankal, D. Adhyaru, Bacterial foraging optimization algorithm: aderivative free technique, in: Proceedings of the Nirma University International Conference on Engineering (NUiCONE), Gujarat, India, 2011, 8–10 December.

[53] A.K. Kar, Bio inspired computing–a review of algorithms and scope of applications, Expert Syst. Appl. 59 (2016) 20–32.

[54] Y. Ma, J. Ru, M. Yin, H. Chen, W. Zheng, Electrochemical modeling and parameter identification based on bacterial foraging optimization algorithm for lithium-ion batteries, J. Appl. Electrochem. 46 (2016) 1119–1131.

[55] H. Han, H. Xu, Z. Yuan, Y. Zhao, State of charge estimation of li-ion battery in evs based on second order sliding mode observer, in: Proceedings of the IEEE Transportation Electrification Conference & Expo 2014 (ITEC Asia-Pacific), Beijing, China, 2014, 31 August–3 September.

[56] W. Wang, H.S.H. Chung, J. Zhang, Near-real-time parameter estimation of an electrical battery model with multiple time constants and SoC-dependent capacitance, IEEE Trans. Power Electron. 29 (2014) 5905–5920.

[57] H.H. Afshari, M. Attari, R. Ahmed, M. Farag, S. Habibi, Modeling, parameterization, and state of charge estimation of li-ion cells using a circuit model, in: Proceedings of the Transportation Electrification Conference and Expo (ITEC), Dearborn, MI, USA, 2016, 27–29 June.

[58] Z. Yu, L. Xiao, H. Li, X. Zhu, R. Huai, Model parameter identification for lithium batteries using the coevolutionary particle swarm optimization method, IEEE Trans. Ind. Electron. 64 (2017) 5690–5700.

[59] X. Hu, H. Yuan, C. Zou, Z. Li, L. Zhang, Co-estimation of state of charge and state of health for lithium-ion batteries based on fractional-order calculus, IEEE Trans. Veh. Technol. 67 (2018) 10319–10329.

[60] H. Aung, K.S. Low, J.J. Soon, State-of-charge estimation using particle swarm optimization with inverse barrier constraint in a nanosatellite, in: Proceedings of the Industrial Electronics and Applications (ICIEA), Auckland, New Zealand, 2015, 15–17 June.

[61] M. Ye, H. Guo, B. Cao, A model-based adaptive state of charge estimator for a lithium-ion battery using an improved adaptive particle filter, Appl. Energy 190 (2017) 740–748.

[62] Y. Kishor, C.H. Kamesh Rao, R.N. Patel, L.K. Sahu, An architectural and control overview of DC-microgrid for sustainable remote electrification, Singh, V.K., Bhoi, A.K., Saxena, A., Zobaa, A.F., Biswal, S.. Renewable Energy and Future Power Systems. Energy Systems in Electrical Engineering, Springer, Singapore, 2021.

[63] A. Sreeram, Y. Kishor, C.H. Kamesh Rao, R.N. Patel, Modeling and simulation of SoC-based BMS for stand-alone solar PV-fed DC microgrids. Enabling Methodologies for Renewable and Sustainable Energy, CRC Press, 2023, pp. 1–31. Edition1st EditioneBook ISBN9781003272717.

[64] Y. Kishor, R.N. Patel, PV-battery fed two-stage non-isolated buck-boost converter for low-voltage DC-microgrid, in: Proceedings of the IEEE 2nd International Conference on Smart Technologies for Power, Energy and Control (STPEC), Bilaspur, Chhattisgarh, India, 2021, pp. 1–6.

[65] Sarmah, S.B.; Kalita, P.; Garg, A.; Niu, X.D.; Zhang, X.W.; Peng, X.; Bhattacharjee, D. A Review of State of Health Estimation of Energy Storage Systems: Challenges and Possible Solutions for Futuristic Applications of Li-Ion Battery Packs in Electric Vehicles. J. Electrochem. Energy Convers. Storage **2019**, 16, 040801.

[66] Liu, S.; Cui, N.; Zhang, C. An Adaptive Square Root Unscented Kalman Filter Approach for State of Charge Estimation of Lithium-Ion Batteries. Energies **2017**, 10, 1345.

[67] Miao, Y.; Gao, Z. Estimation for state of charge of lithium-ion batteries by adaptive fractional-order unscented Kalman filters. Energy Storage **2022**, 51, 104396.

[68] Linghu, J.; Kang, L.; Liu, M.; Luo, X.; Feng, Y.; Lu, C. Estimation for state-of-charge of lithium-ion battery based on an adaptive high-degree cubature Kalman filter. Energy **2019**, 189, 116204

[69] Xia, B.; Chen, C.; Tian, Y.; Sun, W.; Xu, Z.; Zheng, W. A novel method for state of charge estimation of lithium-ion batteries using a nonlinear observer. J. Power Sources **2014**, 270, 359–366.

[70] Gruosso, G.; Gajani, G.S.; Ruiz, F.; Valladolid, J.D.; Patino, D. A Virtual Sensor for Electric Vehicles' State of Charge Estimation. Electronics **2020**, 9, 278.

[71] T. Ikeya et al. Multi-step constant-current charging method for an electric vehiclnickel/metal hydride battery with high-energy efficiency and long cycle life. Journal of Power Sources 105. 2002: 6–12

[72] R. Xiong et al.: Critical Review on the Battery State of Charge Estimation Methods for Electric Vehicles. 2018. Vol 6: 1833-1843

[73] Bukhari et al. Comparison of Characteristics - Lead Acid, Nickel Based, Lead Crystal and Lithium Based Batteries. 2017: 444-450

[74] Kim J, Oh J, Lee H. Review on battery thermal management system for electric vehicles. Applied Thermal Engineering 149. 2019:192-212

[75]. D. Linden, "Thomas. B Reddy, Handbook of Batteries," ed: McGraw Hill, New York, 2002.

[76] I. Buchmann, "Batteries in a portable world. 2007," Richmond: CadexElectronics, 2010.

[77] D. Pavlov, Lead-acid batteries: science and technology: Elsevier, 2011.

[78] D. Berndt and D. Berndt, Maintenance-free batteries: lead-acid, nickel/cadmium, nickel/metal hydride: a handbook of battery technology: Research Studies Press, 1997.

[79] D. H. Doughty, P. C. Butler, A. A. Akhil, N. H. Clark, and J. D. Boyes,"Batteries for large-scale stationary electrical energy storage,"TheElectrochemical Society Interface, vol. 19, no. 3, pp. 49-53, 2010.

[80] T. P. Crompton, Battery reference book: Elsevier, 2000.

[81]G. Pistoia, Battery operated devices and systems: From portable electronics to industrial products: Elsevier, 2008.

[82] J. Jiang and C. Zhang, Fundamentals and applications of lithium-ion batteries in electric drive vehicles. John Wiley & Sons, 2015.

[83] R. Korthauer, "Areas of activity on the fringe of lithium-ion battery development, production, and recycling," in Lithium-Ion Batteries: Basics and Applications: Springer, 2018, pp. 249-251.

[84] M. E. Spahr et al., "Purely hexagonal graphite and the influence of surfacemodifications on its electrochemical lithium insertion properties," Journal of The Electrochemical Society, vol. 149, no. 8, pp. A960-A966, 2002.

[85] J. Garche, C. K. Dyer, P. T. Moseley, Z. Ogumi, D. A. Rand, and B. Scrosati, Encyclopedia of electrochemical power sources. Newnes, 2013.

[86] "Knovel–kHTMLViewer" https://app.knovel.com/web/view/khtml/show.v/rcid:kpBRBE0001/cid:kt00BJW6Y1/viewerType :kh tml//root_slug:battery-reference-book/url_ slug:constant-current-charging?kpromoter=Summon&page=3&view=collapsed&zoo m=1) . app.knovel.com. Retrieved 2019-05-11.

[87] C.-H. Lin et al., "Fast charging technique for Li-Ion battery charger," in 200815th IEEE International Conference on Electronics, Circuitsand Systems, 2008, pp. 618-621: IEEE.

[88] Q. Gong, "Modeling study of a vehicle traction battery model," Chinese LABAT Man, vol. 42, no. 2, p. 76, 2005.

[89] M. Ceraolo, "New dynamical models of lead-acid batteries," IEEEtransactions on Power Systems, vol. 15, no. 4, pp. 1184-1190, 2000.

[90] F. M. González-Longatt, "Circuit based battery models: A review," inCongreso Iberoamericano de estudiantes De Ingenieria Electrica. Cibelec, 2006.

[91] H. Fakham, D. Lu, and B. Francois, "Power control design of a battery charger ina hybrid active PV generator for load-following applications," IEEETransactions on Industrial Electronics, vol. 58, no. 1, pp. 85-94, 2010.

[92] H. He, R. Xiong, J. Fan, Evaluation of lithium-ion battery equivalent circuit models for state of charge estimation by an experimental approach, Energies 4 (4) (2011) 582–598.

[93] A. Hentunen, T. Lehmuspelto, J. Suomela, Time-domain parameterextraction method for thévenin-equivalent circuit battery models, ieee transactions on energy conversion 29 (3) (2014) 558–566

[94] Linden, D., & Reddy, T. B. (Eds.). (2002). Handbook of batteries (3rd ed.). McGraw-Hill.

[95] Arora, P., & Zhang, Z. (2004). Battery materials for ultrafast charging and discharging. Nature, 430(7000), 657-661.

[96] Tarascon, J. M. (2010). Is lithium the new gold? Nature chemistry, 2(6), 510-510

[97] Whittingham, M. S. (2004). Lithium batteries and cathode materials. Chemical reviews, 104(10), 4271-4301.

[98] Scrosati, B., & Garche, J. (2010). Lithium batteries: Status, prospects and future. Journal of Power Sources, 195(9), 2419-2430

[99] Doyle, Marc, Thomas F. Fuller, and John Newman. "Modeling of galvanostatic charge and discharge of the lithium/polymer/insertion cell." Journal of the Electrochemical Society 140.6 (1993): 1526-1533.

[100] Newman, John, and Kai Yu. "Modeling of galvanostatic charge and discharge of the lithium/polymer/insertion cell." Journal of the Electrochemical Society 140.3 (1993): 922-927.

[101] Ramadesigan, Venkatasailanathan, et al. "Modeling and simulation of lithium-ion batteries from a systems engineering perspective." Journal of the Electrochemical Society 159.3 (2012): R31-R45.

[102] Smith, Kandler, et al. "Accurate electrical battery model capable of predicting runtime and I-V performance." Journal of Power Sources 136.2 (2004): 303-312.

[103] D. Doerffel and S. A. Sharkh, "A critical review of using the Peukert equation for determining the remaining capacity of lead-acid and lithium-ion batteries," Journal of power sources, vol. 155, no. 2, pp. 395-400, 2006.

[104] G. Albright, J. Edie, and S. Al-Hallaj, "A comparison of lead acid to lithium-ion in stationary storage applications," Published by AllCell Technologies LLC, 2012.

[105] H. Chang and H. Wu, "Graphene-based nanocomposites: preparation,functionalization, and energy and environmental applications," Energy & Environmental Science, vol. 6, no. 12, pp. 3483-3507, 2013.

[106] H. Keshan, J. Thornburg, and T. S. Ustun, "Comparison of lead-acid and lithium ion batteries for stationary storage in off-grid energy systems," 2016.

[107] E. M. Krieger, J. Cannarella, and C. B. Arnold, "A comparison of lead-acid and lithiumbased battery behavior and capacity fade in off-grid renewable charging applications," Energy, vol. 60, pp. 492-500, 2013.

[108] Ng, K.S.; Moo, C.-S.; Chen, Y.-P.; Hsieh, Y.-C. Enhanced coulomb counting method for estimating state-of-charge and state-ofhealth of lithium-ion batteries. Appl. Energy **2009**, 86, 1506–1511.

[109] Zine, B.; Marouani, K.; Becherif, M.; Yahmedi, S. Estimation of Battery Soc for Hybrid Electric Vehicle using Coulomb Counting Method. Int. J. Emerg.Electr. Power Syst. **2018**, 19.

[110] Baroody, R. UNLV Theses, Dissertations, Professional Papers, andCapstones; UNLV: Las Vegas, NV, USA, 2009.

[111] Mohammed, N.; Saif, A.M. Programmable logic controller based lithium-ion battery management system for accurate state of charge estimation.Comput.Electr.Eng. **2021**, 93, 107306 .

[112] Junping, W.; Quanshi, C.; Binggang, C. Support vector machine based battery model for electric vehicles. Energy Convers. Manag. **2006**, 47, 858–864.

[113] Feng, F.; Lu, R.; Zhu, C. A Combined State of Charge Estimation Method for Lithium-Ion Batteries Used in a Wide Ambient Temperature Range. Energies**2014**, 7, 3004–3032.

[114] Zhang, S.; Guo, X.; Dou, X.; Zhang, X. A data-driven coulomb counting method for state of charge calibration and estimation of lithium-ion battery. Sustain. Energy Technol. Assessments **2020**, 40, 100752.

[115] Gismero, A.; Schaltz, E.; Stroe, D.-I. Recursive State of Charge and State of Health Estimation Method for Lithium-Ion Batteries Based on Coulomb Counting and Open Circuit Voltage. Energies **2020**, 13, 1811.

[116] Hinz, H. Comparison of Lithium-Ion Battery Models for Simulating Storage Systems in Distributed Power Generation. Inventions **2019**, 4, 41.

[117] Tremblay, O.; Dessaint, L.-A.; Dekkiche, A.-I. A Generic Battery Model for the Dynamic Simulation of Hybrid Electric Vehicles. In Proceedings of the IEEE Vehicle Power and Propulsion Conference, Arlington, TX, USA, 9–12 September 2007; pp. 284–289.

[118] Ren, G.; Wang, H.; Chen, C.; Wang, J. An energy conservation and environmental improvement solution-ultra-capacitor/battery hybrid power source for vehicular applications. Sustain. Energy Technol. Assess. **2021**, 44, 100998

[119] Coleman, M.; Lee, C.K.; Zhu, C.; Hurley, W.G. State-of-charge determination from EMF voltage estimation: Using impedance, terminal voltage, and current for lead-acid and lithium-ion batteries. IEEE Trans. Ind. Electron. **2007**, 54, 2550–2557.

العنوان: انجاز مقدر لحالة شحن بطارية السيارة الكهربائية.

الملخص:

يعد التقدير الدقيق لحالة الشحن (SOC) في بطاريات الرصاص الحمضية أمرًا بالغ الأهمية لتحسين نطاق القيادة وضمان التشغيل الآمن للسيارات الكهربائية. ولتحقيق هذه الغاية، تم تطوير العديد من نماذج البطاريات لنمذجة السلوكيات الكهروكيميائية المعقدة والتنبؤ بـ SOC لبطاريات الرصاص الحمضية. ومع ذلك، فإن العديد من هذه النماذج تتطلب حوسبة مكثفة أو تتطلب تحديد معلمات معقدة، مما يشكل تحديات أمام التنفيذ في الوقت الفعلي في تطبيقات السيارات.

تهدف هذه الأطروحة إلى تطوير نموذج بطارية بسيط وفعال مصمم للتكامل مع أنظمة المركبات الكهربائية. يستفيد النموذج المقترح من طريقة عد الكولوم الراسخة، حيث يتم تقدير SOC من خلال تتبع تدفق الشحنة التراكمية خلال سلسلة من دورات الشحن والتفريغ. ومن خلال استخدام هذه التقنية، يمكن للنموذج تقديم تقديرات موثوقة لـ SOC مع تقليل النفقات الحسابية، مما يمهد الطريق لاستراتيجيات إدارة البطارية الذكية في السيارات الكهربائية.

الكلمات المفتاحية: حالة الشحن، سيارة كهربائية، بطاريات الرصاص الحمضية، نموذج البطارية، طريقة عد كولوم.

Titre : Réalisation d'un estimateur de l'état de charge de la batterie d'un véhicule électrique.

Résumé :

Une estimation précise de l'état de charge (SOC) des batteries au plomb est cruciale pour améliorer l'autonomie et garantir un fonctionnement sûr des véhicules électriques. À cette fin, plusieurs modèles de batteries ont été développés pour modéliser les comportements électrochimiques complexes et prédire le SOC des batteries au plomb. Cependant, bon nombre de ces modèles nécessitent des calculs intensifs ou nécessitent un paramétrage complexe, ce qui pose des défis pour la mise en œuvre en temps réel dans les applications automobiles.

Cette thèse vise à développer un modèle de batterie simple mais efficace conçu pour être intégré aux systèmes de véhicules électriques. Le modèle proposé tire parti de la méthode de calcul coulombienne bien établie, dans laquelle le SOC est estimé en suivant le flux de charge cumulé sur une série de cycles de charge et de décharge. En utilisant cette technique, le modèle peut fournir des estimations fiables du SOC tout en réduisant les frais de calcul, ouvrant ainsi la voie à des stratégies intelligentes de gestion des batteries dans les véhicules électriques.

Mots clés : Etat de Charge (SOC), Véhicule Electrique,batteries au plomb est cruciale , Modèle générique de Batterie, Méthode de Comptage Coulométrique.

Title: Create an estimate of the state of charge of an electric vehicle battery.

Abstract:

Accurate estimation of the state of charge (SOC) in lead-acid batteries is crucial for optimizing the driving range and ensuring safe operation of electric vehicles. To this end, numerous battery models have been developed to model the complex electrochemical behaviors and predict the SOC of lead-acid batteries. However, many of these models are computationally intensive or require intricate parameterization, posing challenges for real-time implementation in automotive applications.

This thesis aims to develop a simple yet effective battery model tailored for integration with electric vehicle systems. The proposed model leverages the well-established coulomb counting method, wherein the SOC is estimated by tracking the cumulative charge flow during a series of charge and discharge cycles. By employing this technique, the model can provide reliable SOC estimates while minimizing computational overhead, paving the way for intelligent battery management strategies in electric vehicles.

Keywords: State of Charge (SOC), Electric Vehicle, Lead-Acid Batteries, Battery Generic Model, Coulomb Counting Method.